Electronic Theses and Dissertations, 2004-2019

2018

# Investigation into the Feasibility of Adding Turbulators to Rocket Combustion Chamber Cooling Channels Using a Conjugate Heat Transfer Analysis

Tyler Buchanan
*University of Central Florida*

INVESTIGATION INTO THE FEASIBILITY OF ADDING TURBULATORS TO ROCKET
COMBUSTION CHAMBER COOLING CHANNELS USING A CONJUGATE HEAT
TRANSFER ANALYSIS

by

TYLER SCOTT BUCHANAN

B.S.M.E., University of Central Florida, Orlando, 2016

A thesis submitted in partial fulfillment of the requirements
for the degree of Master of Science in Mechanical Engineering
in the Department of Mechanical and Aerospace Engineering
in the College of Engineering and Computer Science
at the University of Central Florida
Orlando, Florida

Summer Term

2018

Major Professor: Jayanta Kapat

# ABSTRACT

A conjugate heat transfer analysis will be carried out to simulate an 89 kN thrust chamber hydrogen cooling channel, to determine the feasibility of adding turbulators to the combustion chamber cooling channels at various parameters such as angle, pitch, and height of the turbulator. An existing regeneratively cooled chamber environment is simulated and used as a baseline case to be compared against. The new design includes using ribbed turbulators or delta wedges in the cooling channels to increase the heat transfer on the channel hot wall (wall adjacent to the hot gas wall) and on the two channel sidewalls. With a higher heat transfer coefficient, the sidewalls behave like fins for heat transfer and participate more in the overall heat transfer process in the channel. Efficient rib and wedge geometries are chosen based on previous investigations. A conjugate heat transfer analysis is performed using a straight duct with the rib and wedge geometries included, with boundary conditions similar to those found in the combustion chamber, to provide thermal hydraulic performance data at numerous turbulator configurations. The baseline channel's maximum hot wall temperature is the target maximum hot wall temperature that is desired to be reduced. The goal is to reduce the hot gas side wall temperature at a minimal cost in pressure drop.

# ACKNOWLEDGMENTS

# TABLE OF CONTENTS

# LIST OF FIGURES

# LIST OF TABLES

# NOMENCLATURE

$h_{hg}$    = Hot Gas Heat Transfer Coefficient

$T_{aw}$    = Adiabatic Wall Temperature

$T_{hgw}$   = Hot Gas Wall Temperature

$k$       = Channel Wall Thermal Conductivity

$T_{cw}$    = Channel Wall Temperature

$T_{cw}$    = Channel Wall Temperature

$T_{c,\infty}$   = Channel Freestream Temperature

$T_{hg,\infty}$  = Hot Gas Freestream Temperature

$T_{0,hg}$  = Hot Gas Stagnation Temperature

$k$       = Channel Wall Thermal Conductivity

$T_{cw}$    = Channel Wall Temperature

$T_{cw}$    = Channel Wall Temperature

$T_{c,\infty}$   = Channel Freestream Temperature

$T_{hg,\infty}$  = Hot Gas Freestream Temperature

$T_{0,hg}$  = Hot Gas Stagnation Temperature

$P$       = Perimeter

$A_c$     = Cross-sectional Area

$q''_{hg}$    = Hot Gas Heat Flux

$q''_{cond}$  = Heat Flux Through Channel

$q''_c$     = Coolant Wall Heat Flux

$q''_{sw}$    = Sidewall Heat Flux

# ABBREVIATIONS

AR       = Aspect Ratio

CC       = Combustion Chamber

DMLS  = Direct Metal Laser Sintering

HTC    = Heat Transfer Coefficient

H        = Height of Channel

D.h      = Hydraulic Diameter

LRE    = Liquid Rocket Engine

P        = Pitch

e        = Rib Height

SLM    = Selective Laser Melting

# CHAPTER 1: INTRODUCTION

## 1.1 History of Rocketry

Rocketry has enabled humans to reach the moon, and regularly access orbital positions around the Earth. It has enabled manmade research vehicles to reach beyond the moon to orbit, and land on, other planets and bodies in our solar system. It has even enabled manmade vehicles to leave our solar system. Continually improving the technology of rocketry will allow all the aforementioned accomplishments to become commonplace and allow for future missions to reach every corner of our solar system, and further.

Robert Goddard built and flew the first liquid fueled rocket in 1926 [1]. He was first to apply the de Laval nozzle (convergent-divergent (CD) nozzle) to a flow for the purpose of thrust. Without the CD nozzle, rocket engines simply would not work, as they wouldn't be nearly as powerful as they are with a CD nozzle, and the supersonic flow in the engine would not be possible. With thrust being equal to the mass flow rate times the velocity of the fluid, the CD nozzle allowed the fuel and oxidizer products to be accelerated to an exhaust velocity which would never be possible without it. Robert was not able to design and build robust pump systems for his early rockets, but that technology would be developed over the rest of the twentieth century. His first rockets used tank feed pressure systems to pressurize fuel and oxidizers. His contributions laid the foundation for rocketry to begin its growth into what we know it as today.

**Figure 1: Robert Goddard with his first liquid fueled rocket [1]**

In 1923 Goddard integrated regenerative cooling into an engine. He then dismissed the idea as being too complex. This is ironic since nearly every liquid rocket manufactured today utilizes regenerative cooling for some to all of their active cooling. Regenerative cooling is such a vital part of modern rocketry that many engine's nozzles are made completely out of cooling channels.

From the V2 rockets used during WWII to the rockets made by the Americans and the Soviets during the space race, most have been expendable one way or another. With governments being the primary customer, cost was secondary to performance. This resulted in expendable engines and vehicles becoming the low hanging fruit when it came to putting humans and cargo into space. Technical difficulties also contributed to rockets becoming expendable during this era. It would have required much more time to research methods to fully reuse the rocket engines of the day. Some of these additional difficulties include taking

a body that could be traveling 5000+ km/hr and reversing its course. Reentry itself is a process which subjects a vehicle to extreme environments. As far as the engines go, full reusability requires a more robust design so the life of the components allow for reusability under the extreme conditions that an engine experiences.

The United States' Space Shuttle was a large-scale attempt to reuse rocket engines and the entire vehicle. The Shuttle vehicle was made largely reusable thanks to the thermally insulating tiles applied all over its body. These protected the Shuttle and its crew from the high temperatures associated with reentry. The Space Shuttle Main Engines (SSME) were made to be very robust. Still, they needed to be thoroughly inspected between flights and often needed parts to be replaced and/or refurbished [2]. A contributing factor to increasing the reusability of the engines was the type of fuel they used. The SSME's used liquid hydrogen and liquid oxygen for its propellants. The hydrogen was made to run through cooling channels in the nozzle and combustion chamber to cool it. The nozzle was made of the cooling channels. They served a double purpose, to act as a CD nozzle and to maintain the nozzle wall temperature in an allowable range. An additional benefit of this method of cooling is that after the fuel absorbs energy from the hot gas environment through the nozzle wall, it then burns it to power the turbopumps. This reusing of the energy absorbed through cooling is why this method of cooling is called regenerative cooling. This will be addressed in greater detail later. Novel cooling methods like this are required to keep materials within their structural safety limits.

In more recent years, there has been a push to drive down the cost of putting mass into space. New competition in space flight providers has led to this renewed goal. An increasing

number of companies are attempting to put mass into orbit, and some are trying to go further. Many companies are trying various approaches to reduce the cost to place payloads in orbit.

Reusability is believed to be one of the greatest ways to reduce the costs of operating a space transportation service. Cost saving is probably the greatest pro of reusability. Instead of buying X number of new engines that cost Y millions of dollars for each launch, use those engines for 2, 3, or more launches. This is easier said than done however. When an engine is expendable, the design reflects that by planning for an operating life on the order of minutes. The cost of each engine is attempted to be kept to a minimum, but it seems that no amount of cost savings for an engine can justify making it expendable, if reusable engines become a viable option. For reusability, new designs are required that reflect an operating life on the order of hundreds of minutes or more. Some of the most effective ways to increase component life is to reduce mechanical stress and thermal loads. Reducing either of these factors in rocket engines necessitates investigating new methods of operation and manufacturing. There are techniques that may have been known in the past to improve life or performance, but may not have been justified on an expendable engine. For instance, in the past when it was desired to keep a nozzle wall below a certain temperature, the groups involved may have opted to use methods that are typically acceptable for one flight engines, such as ablative cooling, instead of more complex systems like regenerative or film cooling, which could be used on more than one flight.

## 1.2 Rocket Engine Cycles

For liquid rocket engines, there are three primary types of engine cycles, expander, gas generator, and staged combustion figures 2, 3, & 4, respectively. These cycles are defined by what path the propellants take through the engine and by the method used to drive the turbine.

4

There are advantages to each engine, for instance, the three engine types vary in cost, complexity, efficiency, power, and others. All cycles provide a method to run a compressor so the desired chamber pressure can be maintained. Specific impulse (Isp) is how an engines efficiency is measured. It tells how much thrust is achieved per unit of propellant mass used.
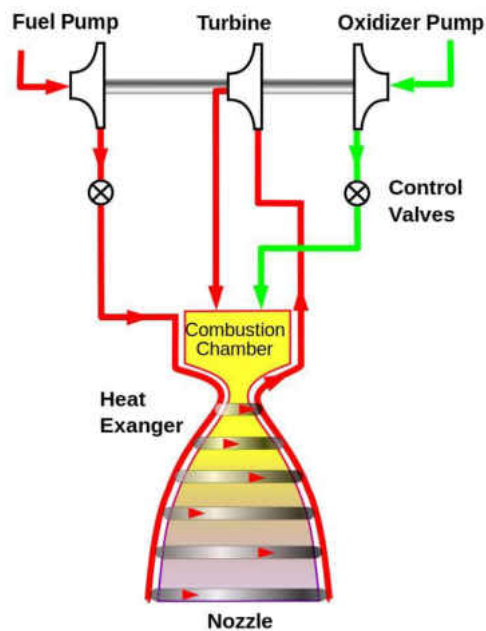


**Figure 2: Expander Cycle LRE [3]**
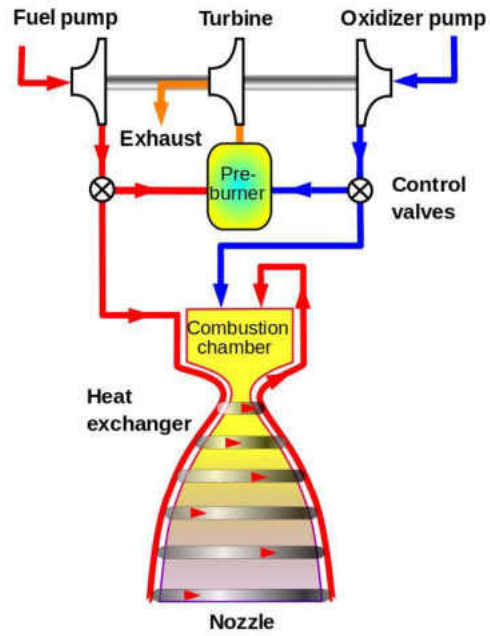
**Figure 3: Gas Generator LRE [3]**
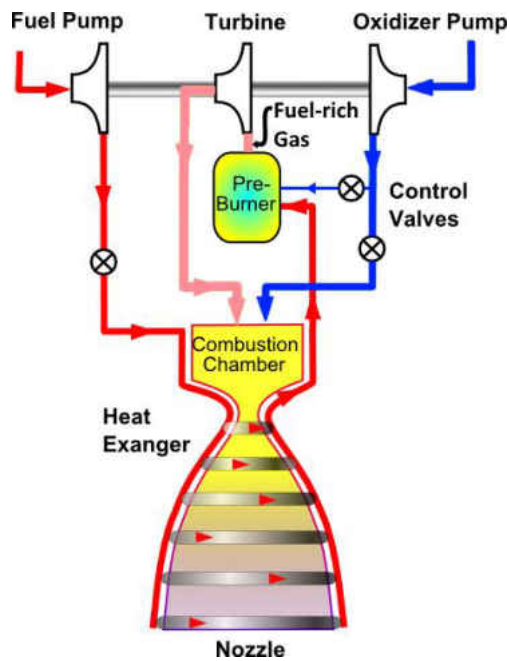


**Figure 4: Staged Combustion LRE [3]**

An expander cycle uses heat picked up from cooling the combustion chamber and nozzle to drive the turbine. Typically, as the fuel runs through regenerative cooling channels its temperature has greatly increased. After exiting these channels, the fuel is then directed to the turbine where it produces the power required to run the compressor. An advantage to this cycle is that it can provide high Isp as the cooling channels are part of a closed system and the coolant is also used as the propellant. Expander cycle engines are limited in the amount of thrust they can provide, at about 300 kN [4]. This is because the nozzle gets larger, the nozzle wall heat exchanger grows by the radius squared and the volume grows by the radius cubed. So, the heat pickup is limited.

A gas generator cycle is where a small amount of propellant is burned upstream of the main combustion chamber. The reactants are then used to drive a turbine, which in turn drives the compressor. A unique feature of this cycle that the other two do not share is that, after the propellant reactants make it across the turbine, it is exhausted out of the engine. This method allows for the engine to be simpler than, and cheaper to manufacture than, expander and staged combustion engines. A drawback to a gas generator cycle is that since the propellant is exhausted overboard and not burned in the main combustion chamber, it typically has a lower Isp than the other two cycles.

A staged combustion cycle is like a gas generator cycle, but instead of dumping the turbine exhaust overboard, it is sent to the main combustion chamber. This way, instead of sending mass and potentially unburned fuel overboard from the turbine exhaust, more energy can be extracted from that mass by burning it further in the main combustion chamber and by increasing the mass flow rate (slightly) through the C-D nozzle. Most configurations of staged combustion cycle engines have either one or two preburners. These are where the initial

combustion occurs to drive the turbine or turbines. This cycle is the most complex of the three to develop but offers higher Isp than a gas generator cycle and higher thrust potential than an expander cycle.

## 1.3 Rocket Cooling Methods

Liquid rocket engines must use novel ways to maintain components within structural limits. The combustion hot gas temperature is higher than the failure point and/or melting point of the combustion chamber and nozzle. Typically, ablation cooling, thermal barrier coatings, film cooling, and regenerative cooling are used to keep the engine cool enough to operate properly.

Ablation cooling is when solid material on the walls sublimes and carries heat away with it. An ablative material is applied to the interior wall of the combustion chamber and/or the nozzle. This kind of treatment is usually intended for a single use. This method does not usually effect Isp or performance of the engine. Due to its wearing away during each use, ablation is not as promising as other cooling methods for reusability.

A thermal barrier coating (TBC) is a very thin layer of material that adheres to the interior wall of the nozzle and/or chamber. This material has low thermal conductivity. Heat travels slowly through a TBC layer, which means that the TBC surface in contact with the nozzle/chamber wall maintains a lower temperature than the side exposed to the hot gas environment. This helps to separate the wall from the hot gas environment. This method does not usually effect Isp or performance. This method of cooling is usually not enough by itself, so other methods of cooling must also be used. If other robust methods of cooling are "good enough" (like regenerative cooling) then TBC isn't applied because then it becomes an extra cost.

Film cooling is when the interior wall of the chamber and/or nozzle is covered by a liquid or gaseous film. This film is "placed" on the wall by specially designed ports within the walls that release the fluid into the flow path in such a way so that it remains on the wall for as long as possible. This layer on the wall serves to separate the wall from the hot gas environment and provides more matter for the heat from the hot gas environment to travel through before it gets to the nozzle/chamber wall. This method can be very effective at maintaining thermal environments, but uses fuel as the film, which means less fuel enters the chamber through the injectors to participate in combustion.

Radiation Cooling is typically used on upper stages of a vehicle. Upper stage engines tend to be smaller than booster engines since most of the weight of the original vehicle is no longer part of the accelerating mass. A nozzle which utilizes radiation as its method of cooling usually weights less also, since it doesn't need to be made to carry high pressure coolant through its walls or adhere ablative material to it. In the low-pressure environment of the upper atmosphere or in orbit larger nozzles are desired to improve thrust and Isp. Larger area ratio nozzles make radiatively cooled nozzles even more advantageous than actively cooled ones. The material is usually made of a metal or carbon composite that is capable of handling high temperatures, beyond the melting point of more frequently used metals. When heated up by the hot gas environment, the heat travels through the nozzle and radiates away from the outer surface. Only the nozzle or nozzle extensions are made to be radiatively cooled in large LRE's as the material it's made of is not strong enough to be used for the combustion chamber. The following section will cover regenerative cooling.

## 1.4 Regenerative Cooling

Regenerative cooling may be the most robust method of cooling of the four mentioned here. Usually fuel, sometimes oxidizer, is flowed through channels that makeup the nozzle/chamber walls including hydrogen, rocket propellent-1 (highly refined kerosene), liquid oxygen, or methane. The coolant comes from the pump system of the engine and can enter from the forward or aft (near nozzle exit plane) part of the engine, as seen in figure 5.
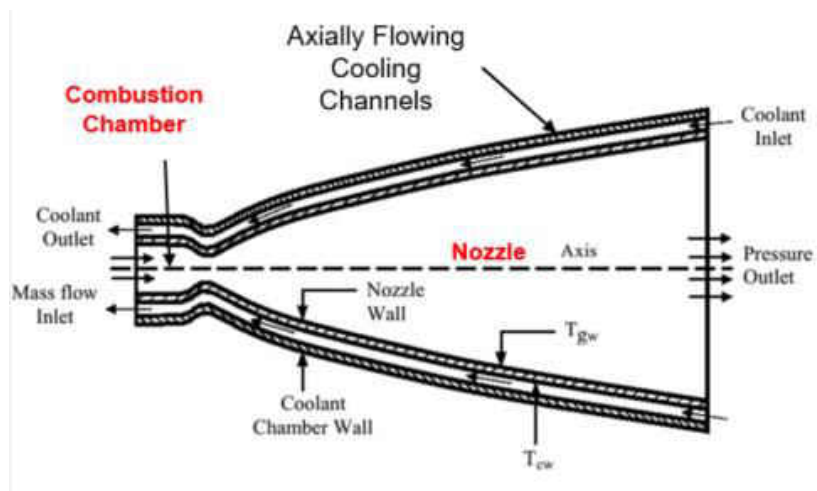


**Figure 5: Diagram of Regeneratively Cooled Nozzle [5]**

The flowrate is fast enough and/or the temperature is low enough that, the wall temperature can be maintained within thermal limits using this method. This method improves Isp over not using it, as all the heat that is drawn out of the chamber/nozzle and picked up by the coolant is then redirected to be used for the main combustion process. This means that heat is not lost through cooling but is recaptured. Except for minor losses, all the energy leaving the energy is through the nozzle, which improves the efficiency. Now that reusability is becoming more desirable in the rocket industry, there is an incentive to improve

the thermal performance of regenerative cooling channels. This investigation aims to study the feasibility of using wedge turbulators in a LRE chamber cooling channel environment to determine if improved thermal performance is possible.

The heat entering the nozzle wall and traveling into the coolant channel can take two paths, directly through the wall into the hot channel wall (channel bottom wall), or through the channel sidewall and into the coolant flow. All variables in the following section can be found in table 1.

**Table 1: Nomenclature for Heat Transfer Equations**

$h_{hg}$ = Hot Gas Heat Transfer Coefficient
$T_{aw}$ = Adiabatic Wall Temperature
$T_{hgw}$ = Hot Gas Wall Temperature
$k$ = Channel Wall Thermal Conductivity
$T_{cw}$ = Channel Wall Temperature
$T_{cw}$ = Channel Wall Temperature
$T_{c,\infty}$ = Channel Freestream Temperature
$T_{hg,\infty}$ = Hot Gas Freestream Temperature
$T_{0,hg}$ = Hot Gas Stagnation Temperature
$k$ = Channel Wall Thermal Conductivity
$T_{cw}$ = Channel Wall Temperature
$T_{cw}$ = Channel Wall Temperature
$T_{c,\infty}$ = Channel Freestream Temperature
$T_{hg,\infty}$ = Hot Gas Freestream Temperature
$T_{0,hg}$ = Hot Gas Stagnation Temperature
$P$ = Perimeter
$A_c$ = Cross-sectional Area
$q''_{hg}$ = Hot Gas Heat Flux
$q''_{cond}$ = Heat Flux Through Channel
$q''_c$ = Coolant Wall Heat Flux
$q''_{sw}$ = Sidewall Heat Flux

Starting with the hot gas environment, the driving temperature for heat transfer is the adiabatic wall temperature. The adiabatic wall temperature can be related to the hot gas environment by a recovery factor, equation (1). From this the adiabatic wall temperature can

be used to determine the heat flux into the chamber/nozzle wall, equation (2). The heat

transfer path through the chamber/nozzle wall itself depends on conduction paths, equation

(3). The path directly into the channel bottom wall also relies on typical convection, equation

(4).

$$r = \frac{T_{aw} - T_{hg,\infty}}{T_{0,hg} - T_{hg,\infty}}$$

(1)

$$q''_{hg} = h_{hg}(T_{aw} - T_{hgw})$$

(2)

$$q''_{wall} = k\frac{(T_{hgw} - T_{cw})}{dx}$$

(3)

$$q''_c = h_c(T_{cw} - T_{c,\infty})$$

(4)

The heat transfer path through the sidewalls can be analyzed like traditional heat transfer

fins. Equation (5) shows the typical fin heat transfer path for an infinitely long fin. The fin

efficiency can be evaluated from equation (6). The dependent values m, $L_c$, and, $\theta_b$ can be seen

in equations (7), (8), and (9), respectively. As the heat transfer coefficient on the sidewall

increases, the fin efficiency goes down. This implies that with an enhanced HTC on the sidewall,

other parameters can be adjusted to bring the fin efficiency back up, such as thickness of the

sidewalls.

$$q''_{sw} = \sqrt{hPKA_c}\,\theta_b$$

(5)

$$e_{fin} = \frac{\tanh mL_c}{mL_c}$$

(6)

$$m = \sqrt{\frac{hP}{KA_c}}$$

(7)

$$L_c = L + \tfrac{1}{2}t$$

(8)

$$\theta_b = T_b - T_\infty$$

(9)

Figure 6 shows a diagram of a regenerative cooling channel to illustrate the potential paths for heat transfer to take.

$$q_{hg}'' = q_{cond}'' = q_c'' + q_{sw}''$$
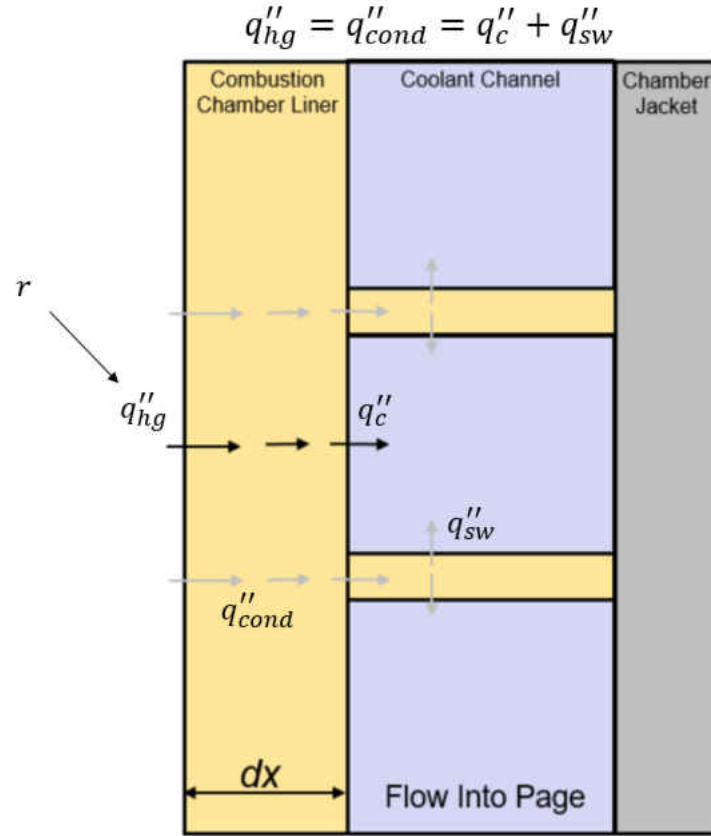


**Figure 6: Heat Transfer Paths of Regenerative Cooling Channels**

The goal is to increase the HTC on the channel bottom wall and the sidewalls by adding turbulators to the channel. This will increase mixing and disrupt the boundary layers that normally exist on the flat channel bottom wall. Figure 7 gives a visualization of the typical thermal gradient in a cooling channel and exaggerated vortices to increase mixing. The vortex vector field equation (10) is the mathematical representation of vortices. For increased mixing it is desired to increase the magnitude of $\vec{\omega}$.

$$\vec{\omega} \equiv \nabla \times \vec{u} = \left( \frac{\partial u_z}{\partial y} - \frac{\partial u_y}{\partial z}, \frac{\partial u_x}{\partial z} - \frac{\partial u_z}{\partial x}, \frac{\partial u_y}{\partial x} - \frac{\partial u_x}{\partial y} \right) \tag{10}$$
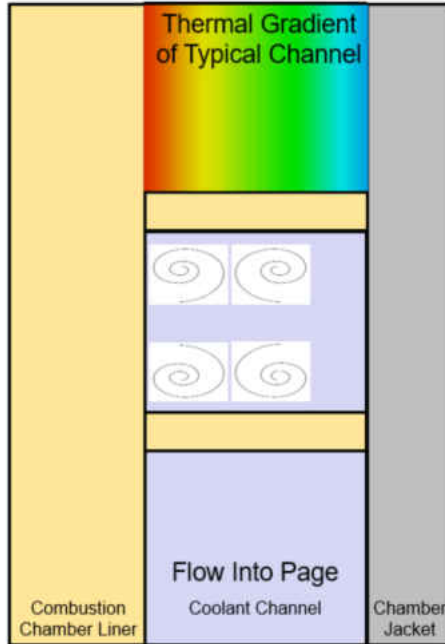
**Figure 7: Regen Cooling Visualization of Typical Thermal Gradient and Desired Mixing**

1.5 Motivation

Lowering the hot gas wall temperature is an effective method to increase the life and reliability of LRE's. Quentmeyer et al [6] investigated the relationship between maximum hot gas wall temperature and cycle fatigue life. Equation (11) explains that relationship $N_f$ is number of cycles to failure and $T_{gw}$ is the hot gas wall temperature. Lowering the maximum hot gas wall temperature effectively increases the low cycle fatigue. If full reusability of LRE is to become a reality, low cycle fatigue will be of great importance.

$$T_{gw} = \frac{5}{9}4520 N_f^{-0.205} \rightarrow N_f = \left(\frac{\frac{9}{5}T_{gw}}{4520}\right)^{-4.87805}$$

(11)

In addition to increasing the life of LRE components, figure 8 illustrates the relationship between coolant wall thickness and heat transfer of the coolant channels, and how they relate to chamber pressure. By increasing the heat transfer of the cooling channels, the heat transfer limit curve is translated to the right, thereby allowing for the ability to increase the cooling channel walls, and in turn increase chamber pressure. Increasing chamber pressure can easily result in more thrust and higher allowable Isp.
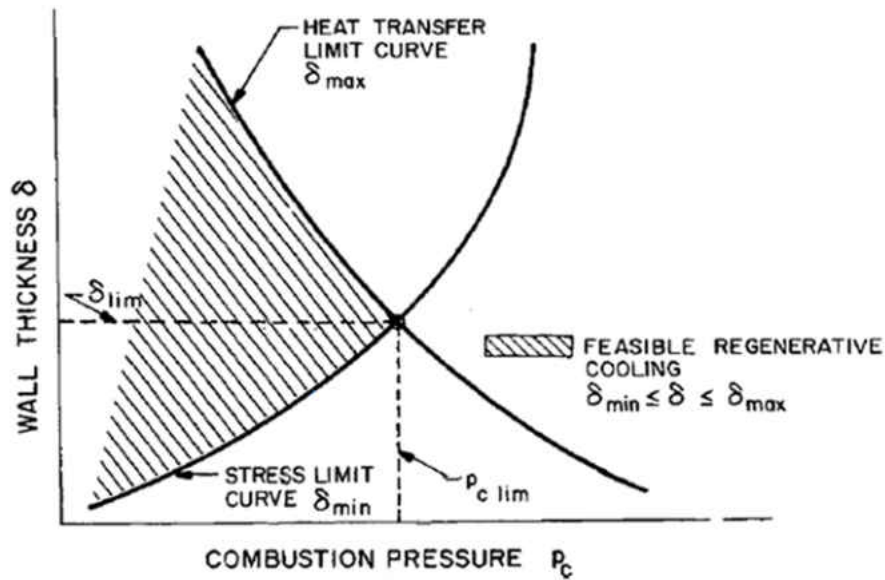


**Figure 8: Coolant Wall Thickness vs Chamber Pressure and Their relationship with Heat Transfer Limits of the Channel [7]**

Due to the changes occurring in the rocket industry, new methods are being investigated to drive towards reusability. This means that new techniques will be researched and techniques from other industries/applications will be utilized to achieve this goal.

The gas turbine industry has had similar challenges to overcome to make gas turbine engines high performance and economical. Like in a rocket engine combustion chamber, first stage turbine blades in a gas turbine are constantly exposed to hot gas temperatures that exceed the melting point of the Inconel blades themselves. That industry has addressed this

16

by coming up with novel ways to keep gas temperatures high and maintaining the structural integrity of the components exposed to it. Figure 9 shows the LRE industry progress compared to the gas turbine industry. Green circles indicate methods utilized by the LRE industry, and red circles indicate techniques utilized by the gas turbine industry but not the LRE industry.
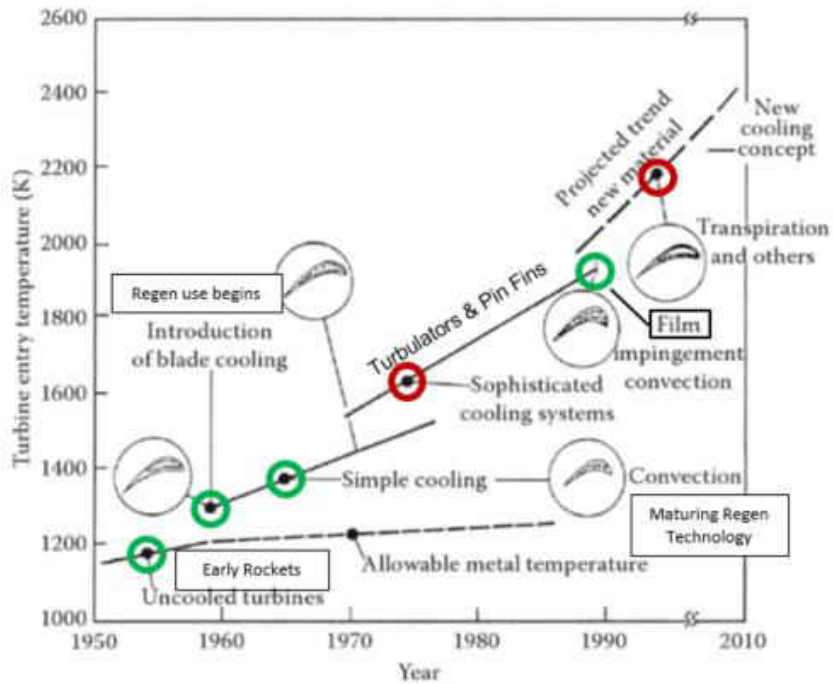


**Figure 9: Gas Turbine and LRE Industry Progress [8]**

Some of these novel heat transfer methods include internal duct cooling in the turbine blades, film cooling on the surface of the turbine blades, pin fin cooling in the trailing edge of the blades, and impingement cooling on the internal surfaces of the blades. The first of these methods, internal duct cooling, is of interest to us because it one of the most adaptable methods for systems other than turbine blades. Internal duct cooling in turbine blades consist of cooling channels running through the internals of the blades. The purpose of adding

17

cooling channels here is to take excess heat out of/ away from the blade structure and prevent overheating.

To make internal duct cooling more effective at removing heat, the gas turbine industry investigated ways to improve the heat transfer rate of those channels. This goal was achieved by adding turbulators to the channels to increase turbulence. Turbulators are variously shaped (ribs, wedges, dimples, etc.) obstructions in the cooling channel/duct. These turbulators then increase the amount of turbulence, and thus mixing, in the channel and increase the heat transfer coefficient on the internal walls of the channel. The cost of this increased thermal performance is an increase in pressure drop. Many factors account for the effectiveness and efficiency of the turbulators thermal performance. The shape, size, amount, and angle of the turbulators all affect the thermal performance. They change the amount, type, and effectiveness of mixing. In addition, the thermal effects of the same geometry turbulator are very different in different environments. For instance, a particular geometry may increase heat transfer with an acceptable pressure drop increase at a low Reynolds number, but that same geometry at a higher Reynolds number may yield prohibitively high pressure drop. All these effects are balanced for optimized performance on the system level. So this method of cooling a gas turbine blade may increase the pressure demands of the compressor portion of the engine, but it enables higher temperatures at the first stage turbine blades, which leads to greater thermal efficiency of the whole system. In gas turbines, despite the increased pressure drop of the cooling channels, there is a net benefit in the overall system.

Liquid rocket engines also use cooling channels in extreme environments. The hot gas temperature in a combustion chamber and nozzle is higher than the melting point of the material that the chamber and nozzle are made of. As mentioned previously, rocket engine

cooling channels have almost all been smooth walled. This has been sufficient in the past, but with increased competition, organizations are now looking at more novel methods for improving their engines. Adding turbulators to cooling channels can potentially be one of those novel methods for increasing engine performance. This investigation aims to study the feasibility of using turbulators in rocket engine cooling channels. The main focus is to determine how much the maximum hot wall temperature can be reduced with the addition of turbulators. This aids in the life of the components, and helps the goal of reusability. Other potential benefits include system level performance improvements. Increasing the amount of heat picked up in the cooling channels allow for new performance regimes, especially in expander cycle engines. There may be many other changes that can improve performance as a result of the increased heat transfer rate in the channel. For instance, if the cooling channel (with turbulators) is picking up more heat than required to maintain hot wall temperatures, perhaps the coolant flow rate can be reduced to yield a more advantageous pressure drop through the channels. This will of course change heat transfer characteristics of the cooling channels and other factors, which means this would have to be an iterative process. Like the gas turbines, there may exist a system balance which has improved performance despite the pressure drop increase that comes with adding turbulators.

Internal cooling through a channel is a very wide field of study. Internal cooling is akin to a regular heat exchanger, where the goal is to decrease (or increase) the amount of energy in a fluid or solid while increasing (or respectively decreasing) the amount of energy in the working fluid. In a rocket engine cooling channel, the goal is to decrease the temperature (energy content) of the chamber and nozzles wall while increasing the amount of energy in the coolant fluid.

High mass flow rates in narrow channels means liquid rocket engine cooling channels have Reynolds numbers on the order of millions. The flow is turbulent as the Reynolds number is well above the typical threshold of 5000 for the transition to turbulent internal flow [9]. The standard heat transfer correlation for turbulent internal flow is the Dittus-Bolter correlation for the Nusselt number. The Dittus-Bolter correlation, equation (12), is not accurate at very high Reynolds numbers [9]. Nu is the Nusselt number, Re is the Reynolds number, and Pr is the Prandtl number. To account for its inaccuracies, other factors are applied to the standard correlation. These include things that are neglected by the Dittus-Bolter correlation, like the ratio of wall density, viscosity, temperature, and pressure, to the core density, viscosity, temperature, and pressure, respectively.

$$Nu_D = 0.023 Re_D^{4/5} Pr^{0.3}$$

(12)

The aerospace industry has challenges that many other industries don't typically need to consider. For instance, for anything that goes into the air, weight is one of the most important factors of the design. Safety is also of paramount concern. Since many aerospace applications involve people, safety usually becomes the most important factor. Failsafe's in the aerospace industry are made to help preserve life in the event of an emergency. Even with a failsafe in place, it is always possible that a failure might lead to an uncontrolled fall back to Earth. These factors make the aerospace industry very conservative when it comes to implementing new technologies and/or methods of operation. To my knowledge, a liquid rocket engine with turbulators used in its cooling channels has not been flown before. This presents increased difficulty, as new technology in the air is viewed with the most scrutiny, rightfully so in the name of safety.

## 1.6 Additive Manufacturing

Up until recently, traditional manufacturing methods have been used to build rocket engines. The amount of human labor required to manufacture rocket engines is astronomical. Also, many engine components require custom made tools to manufacture. The increasing technology behind additive manufacturing and its increasing use in industry are slated to change what manufacturing will look like in the future.

Additive manufacturing has the potential to reduce the costs of rocket engine manufacturing drastically. The cost savings of additive manufacturing comes from greatly reducing the need for human labor and potentially eliminating the need for specialized machines.

Also, as additive manufacturing becomes increasingly relied upon and investigated, new design parameters will be possible. Many geometries exist currently that are extremely expensive or nearly impossible to build, such as, a channel with geometric features on its walls, or an angled pipe or sheet with constant (not strained) structural properties throughout.

Additive manufacturing is the enabling technology this investigation. It allows complex features to be applied to internal cooling channels on a scale which would otherwise be prohibitively expensive, or nearly impossible to make. Even though very small features are now possible, there are still drawbacks to additive manufacturing. One of the limitations with additive manufacturing will always be its resolution. As long as it keeps improving, new applications for it will be realized. At the time of this writing, commercially available resolution for a selective laser melting (SLM) manufacturing process is 20 μm. [10]. It is reasonable to assume that the technology will improve further and that the resolution will continue to improve. Today's current resolution limits are still an improvement over many current manufacturing techniques, for a

given tolerance and price. Figure 10 shows an additively manufactured copper thrust chamber built by NASA, using SLM.



**Figure 10: Additively Manufactured Copper Thrust Chamber [11]**

A challenge of using additive manufacturing is the part's surface roughness after the printing is complete. The surface roughness various depending on the material used and the quality and speed of the printer used. Typically, an additively manufactured part has a higher surface roughness than a traditionally manufactured part. There are processes that can make the surface smoother, but the effectiveness of this varies with material, part geometry, and which method of 3-D printing was used.

# CHAPTER 2: LITERATURE REVIEW

## 2.1 LRE Cooling Channel Studies

There is ongoing research into improving rocket technology. There are several focal points, such as structures, thermal fluids, materials, and more. Within those groups the research focus is further divided into things like, improving current engines/technology, investigating new technologies, improving life, decreasing costs, and more. Much of the relevant research for the current study has to do with improving current engines while looking through a thermal fluid lens. The improvements can potentially improve performance, and/or life of components.

Wadel et al [12] investigated the effects of using very high aspect ratio cooling channels in a combustion/thrust chamber. The study focused on optimizing the cooling channel aspect ratio in the axial direction. The aspect channels ranged from 2.5 to 40. The goal of the study was to reduce the maximum temperature of the hot gas wall.

A measure of used by Wadel to determine the effectiveness of the various designs was the rib effectiveness parameter, equation (13) [12].

$$\varepsilon_r = \left(\frac{2k}{ht}\right)^{1/2} \tag{13}$$

In equation (13), t is the rib thickness, h is the heat transfer coefficient, and k is the thermal conductivity of the rib material. Note that "rib" in this context refers to the cooling channel sidewalls, it does not imply the use of a turbulator. This is a useful metric for Wadel as in some of the channel designs of that study, the channels bifurcated near the throat. This had the effect

of doubling the number of cooling channels near the throat and increasing their aspect ratio. This drove down the t parameter in the rib effectiveness equation, thus increasing the effectiveness value. In the current study, the aspect ratio is constant and the "rib" (channel sidewall) thickness does not change.

The starting point for her study was a baseline channel with a constant aspect ratio of 2.5. Seven other channel designs were simulated. The maximum hot gas wall temperature and associated pressure drop for the baseline case are 764 K and 3.7 MPa, respectively. In the various designs, the aspect ratio changed in the axial direction and some of the designs include bifurcating the channels near the throat.

Wadel's [12] investigation showed that increasing the aspect ratio of cooling channels is an effective way to reduce the maximum hot gas wall temperature. The reduction in hot gas wall temperature for the various cases ranged from 125 K to 164 K. The associated pressure drops for the cases ranged from 3.7 MPa to 5 MPa. Wadel [12] also found that additional balances are possible in thanks to the very high aspect ratio cooling channels. A balance between pressure drop and max hot gas wall temperature could be reached. For instance, if the fin effect of the channel sidewalls is greater, then the mass flow could be reduced to the point where the max hot gas wall temperature is the same as the baseline case but the pressure drop through the channel has decreased due to the lower mass flow rate. There also is the possibility of reducing the mas hot gas wall temperature and reducing the channel pressure drop by balancing all the parameters, such as aspect ratio, bifurcation, mass flow rate, and number of channels.

Another investigation into the aspect ratio of LRE cooling channels was done by Boysan et al [13]. In that study aspect ratios from 0.8 to 8 were investigated. He modeled the cooling channels after the baseline case from Wadel et al [12], then changed the parameters for further study. His

results also concluded that the high aspect ratio cooling channels proved to be more effective at heat transfer than lower aspect ratio ones. However, he did find that high aspect ratio cooling channels only improve heat transfer up to a point, then become less effective, as the area for heat transfer reduces with high aspect ratios. Increasing the number of cooling channels without changing aspect ratios was found to improve heat transfer up to a point then become less effective as more channels are added, due to lower coolant velocity. More channels have a favorable impact on pressure drop also, due to the coolant velocity reduction.

At the time of this writing only one study is known to include turbulators in LRE cooling channels. A study by Hossain [14] was conducted where 90-degree square ribs were placed perpendicular to the stream wise flow of a LRE cooling channel. They made their baseline channel to match Wadel's [12] baseline channel. They placed ribbed turbulators only near the throat, as this is the area of the channel with the highest heat load. Their study found that that the average reduction in the maximum hot gas wall temperature was approximately 36 K with a coolant pressure drop increase of 0.33 percent.

## 2.2 Turbulators

When turbulators were first introduced, 90-degree square wedges [15] were the first geometries studied. They were found to be able to increase the heat transfer coefficient (HTC) on a wall, or walls, of a channel. The cost of the HTC increasing is that the pressure drop through the channel also increases. The relationship between the HTC increase and the pressure drop increase is not fixed, and is different shaped turbulators. Since the first turbulator studies, many geometries have been studied and more efficient turbulators found.

Han et al [15] was among the first to investigate turbulators. The first studies looked into 90 (perpendicular to stream wise flow) degree square ribbed turbulators. His experiments consisted of a channel with isothermal walls and air flowing through. From this he backed out an HTC and a corresponding Nusselt (Nu) number correlation. The 90-degree square ribbed turbulators proved to be able to increase the HTC in a channel, but also greatly increased the channel pressure drop. A later study by Han et al [16] investigated potential ways to improve the efficiency of ribbed turbulators. In this study, he experimented with several different configurations of ribbed turbulators. The designs included using ribs at different angles to the flow (i.e. not 90 degrees), separated (or "broken) ribs, and V shaped ribs with the midplane of the channel acting as a line of symmetry. From these studies, he found that a design using 60-degree V-shaped broken rib configuration performed the best, seen in figure 11. It proved to increase the HTC more efficiently by increasing the number of secondary flows near the channel wall, which improves mixing. It is this rib design that is utilized in the present study for the rib case.



(e) 60° V - shaped broken rib
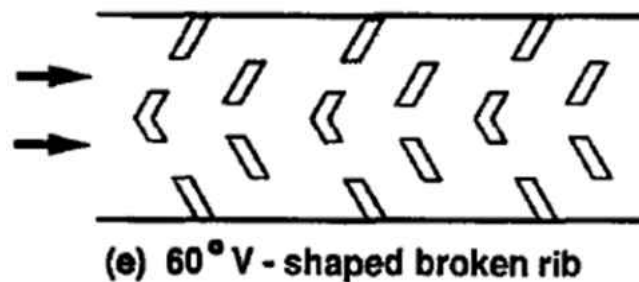
**Figure 11: 60-degree V-shaped broken rib configuration [16]**

It was found that other shaped turbulators can be more effective than ribbed shaped ones. Wedge shaped turbulators were investigated by Han et al [18], and found to be more effective than ribbed turbulators. Similar to the multiple rib configurations studied, Han [18] studied multiple wedge configurations, like continues and broken wedges, and backward facing delta

wedges in different alignments. He found the backward facing delta shaped wedge to be the most efficient at heat transfer enhancement in channels.

Valentino et al [18] studied numerous configurations of backward facing delta wedges in a channel flow. The variations include different size wedges and half wedge shapes. All configurations utilized 60-degree wedges, and one wedge per channel section, as opposed to side by side wedges. More uniform HTC increases came from the whole wedges, which also had a greater overall effect on HTC increases. The initial wedge case of the current study is based on parameters in Valentino's [18] study. The advantages of the backward facing delta wedge come from its ability to efficiently create secondary flow vortices, as seen in figure 12.
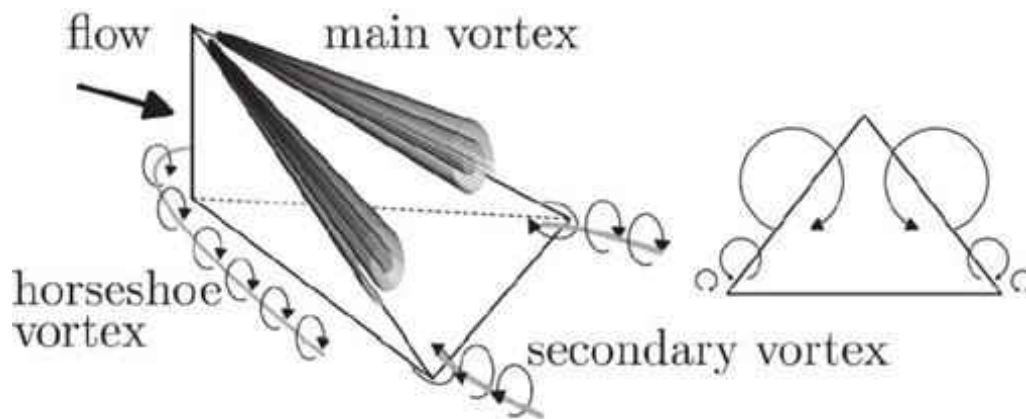


**Figure 12: Backward Facing Delta Wedge Secondary Flows [19]**

# CHAPTER 3: PROBLEM DEFINITION

As competition increases in the rocket industry, more organizations hope to set themselves apart from other manufacturers. To do this, many organizations are looking for ways to make their engines reusable, get more power out of them, and/or increase the overall efficiency of the engine. Since a LRE is a thermal fluid centric system much of the ability to make such improvements can be found in the fluid and/or thermal systems of the engine.

In the present study, an attempt is made to contribute to the above-mentioned improvements by investigating the feasibility of using turbulators in rocket nozzle/combustion chamber cooling channels. The hope is that the results show this to be a valid method to improve the thermal hydraulic performance of such cooling channels and that the topic to be worth further investigation. From this investigation will come a detailed look into the rib case and initial wedge case described later, and a comparison of many different wedge configurations to be compared by their ability to reduce the maximum hot gas wall temperature and their pressure drop penalty.

The current study's baseline model, and by extension, all that follow, is based on the baseline channel design found in Wadel et al [12]. The channel design for that study was based on an 89 kN thrust chamber. The thrust chamber had 100 cooling channels with a total of 2.3kg of hydrogen flowing through them. The combustion environment was simulated. A test thrust chamber was later built and tested using an optimal design as determined from the study.

The first large assumption of the present study is that of constant heat flux into the system. The hot gas wall temperature from the Wadel's [12] baseline case was used as the

boundary condition for the hot gas wall in the current study. From this simulation a hot gas side wall heat flux was determined. This hot gas wall heat flux was then applied to all following cases as the hot gas wall boundary condition. This allows the hot gas wall temperature to change and the various cases to be compared against each other.

The second large assumption of the present study is that of geometric simplification. The Wadel [12] baseline channel that the present study's baseline channel is based on is contoured to match the converging-diverging behavior of the thrust chamber. In the current study, this chamber is represented by a straight channel, as seen in figure 13. This is done to simplify the geometric domain and reduce the computational resources required for the model simulations. It is assumed that the heat transfer difference of the contoured channel compared to the straight channel is negligibly small. The effect of the contour on heat transfer is reduced even more when turbulators are introduced, as they will be the primary drivers in any increasing heat transfer rate. The coolant flows into the inlet which is near the exit plane of the thrust chamber and travels the opposite direction of the hot gas flow.
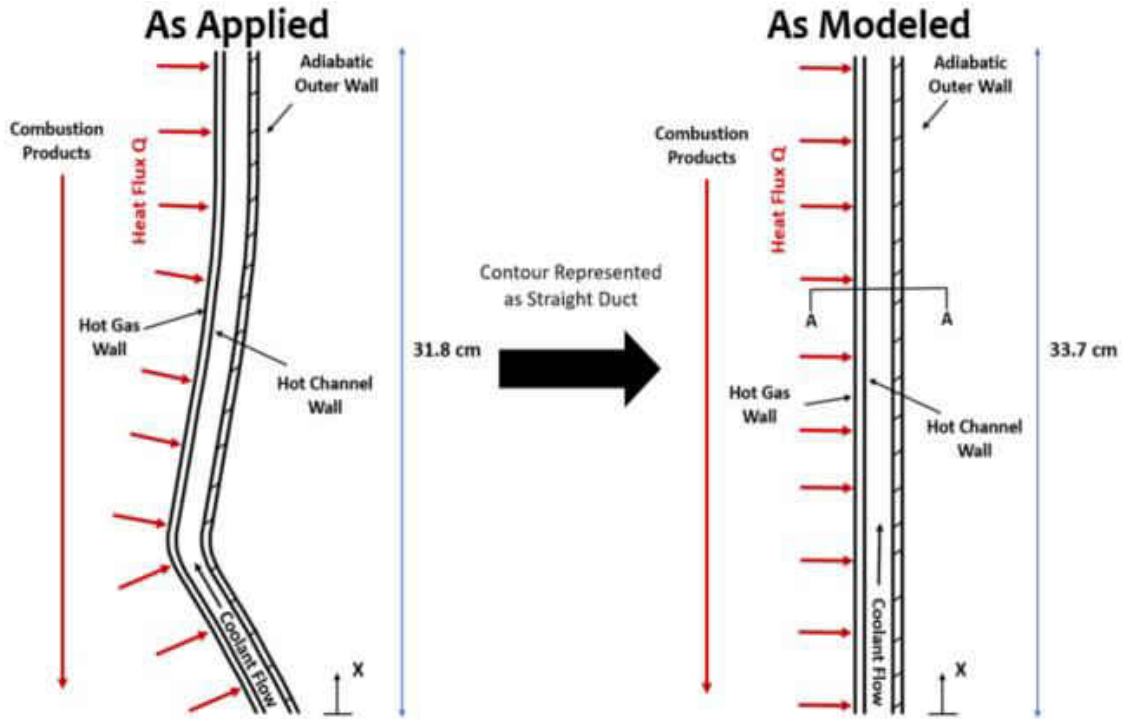
**Figure 13: Cooling Channels as Applied and as Modeled**

The method used to transpose the coordinates of the contoured channel to the straight

channel are based on triangulating the axial distance from the throat and the radius (table 2

shown with point near the inlet). These two parameters are used to determine how far a point is

from the throat, which is then carried over to the straight channel. The throat is point zero,

downstream of the throat (near cooling channel inlet) are positive values, and upstream of the

throat (near cooling channel exit) are negative values. The effect is the straight channel is slightly

longer than the contoured channel as seen in figure 14. The baseline hot gas wall temperature is

then imposed on the straight channel, relative to the throat, the same as the contoured channel.

**Table 2: Method of Transposition from Contour to Straight Channel**

| Distance from Throat | Chamber Radius | Throat Radius |
|:---:|:---:|:---:|
| m | m | m |
| 0.08145 | 0.08491 | 0.03277 |

| x-displacement | y-displacement | Total Displacement |
|:---:|:---:|:---:|
| m | m | m |
| 0.08145 | 0.05214 | 0.09671 |

X-displacement=Distance from Throat

Y-displacement=Chamber Radius-Throat Radius

$$Total\ Displacement = \sqrt{x\ displacement^2 + y\ displacement^2}$$



Near Throat Region for Straight and Contoured Channels

Distance from Throat, cm
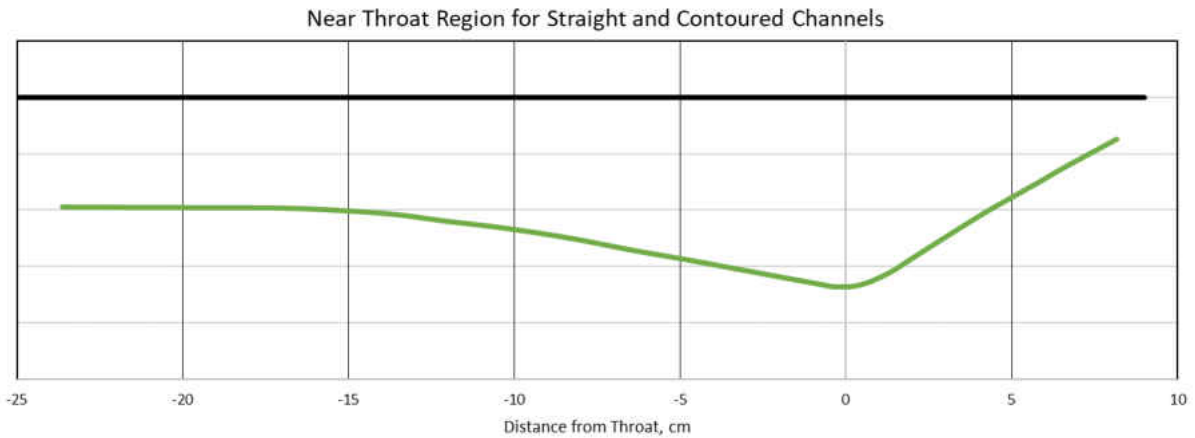
**Figure 14: Contoured and Straight Channel Lengths**

# CHAPTER 4: ANALYSIS OF BASELINE GEOMETRY

A CFD analysis is performed on the baseline case to refine the domain mesh and extract a boundary heat flux. This heat flux is applied as a boundary condition in the following simulations. From each simulation pressure drop and wall temperature will be obtained. Other information such as HTC and mixing can also be obtained from the simulations in order to compare the thermal-hydraulic performance across various runs. The geometry, mesh, boundary conditions, and assumptions about each case is discussed. Results are discussed for each case then compared to one another. All cases were setup, meshed, and run using STAR-CCM+ version 11.06.011 commercial code.

## 4.1 Geometry and Computational Domain

The geometry for the baseline case is made to emulate the baseline case from Wadel's [12] baseline case. The geometry from that study is a convergent-divergent channel, while the current study geometry is represented by a straight channel, as discussed in the previous section. The converging-diverging channel is 31.8 cm in axial length and the straight channel is 33.7 cm in axial length. Figure 15 shows the whole channel baseline geometry. Figure 16 is a cross section of the baseline channel.
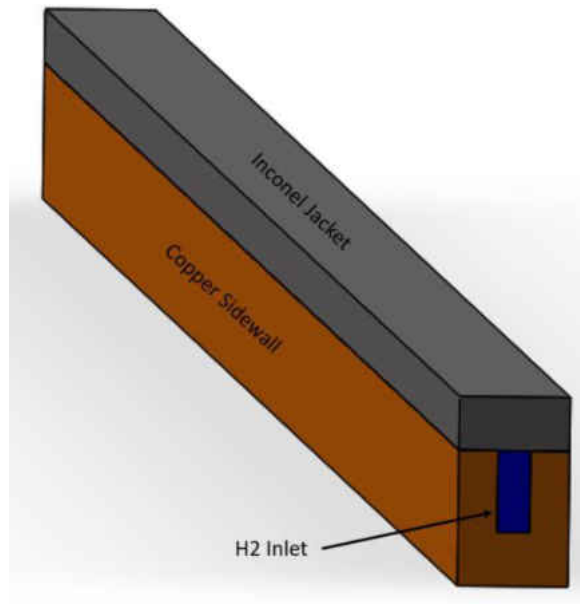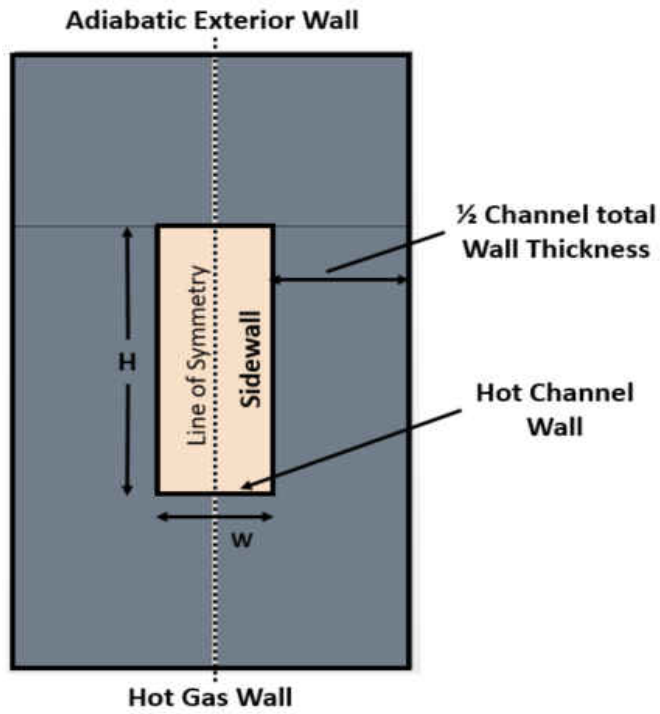
**Figure 15: Entire Baseline Geometry**



**Figure 16: Cross Section of Baseline Channel**

The channel has symmetry along the midplane from top to bottom. To reduce the computational demand, half of the channel is modeled, as seen in figure 17. Channel side and front views can also be seen in figures 18 and 19 respectively. All later geometries are also symmetric along the midplane, so the baseline results can directly be compared to all following cases. The baseline channel is also symmetric along the horizontal midplane halfway up the channel, but the boundary conditions on the top and bottom walls are not the same so it cannot be simplified in that manner. Also, later geometries will not be symmetric on the mid horizontal plane. A point is made to setup and run the baseline case in such a way that later cases require little change to their geometry and mesh.
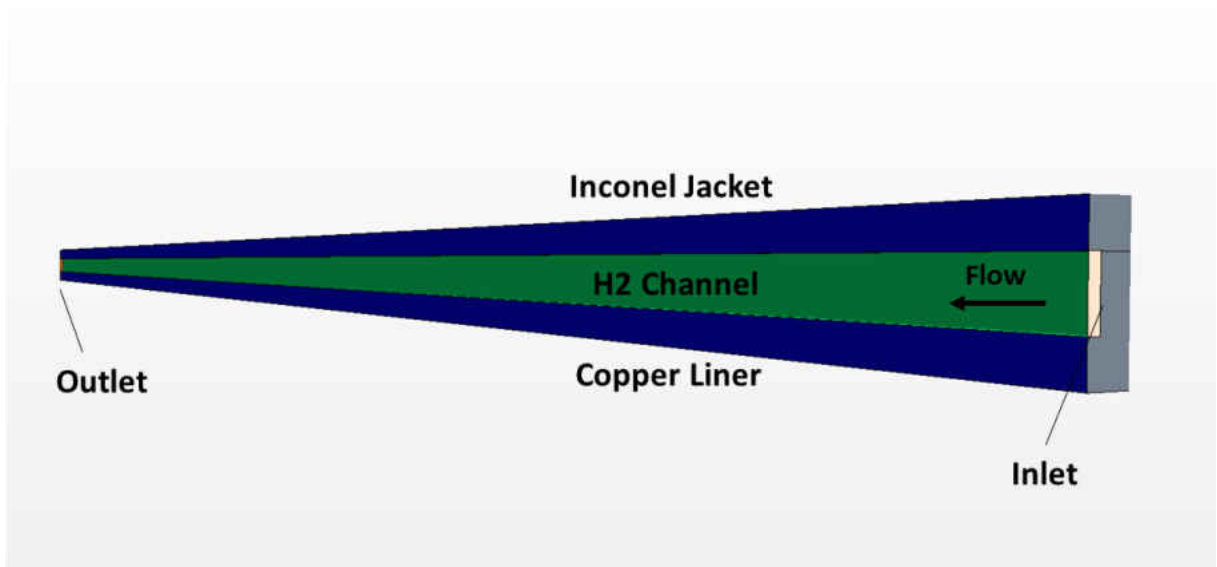


**Figure 17: Baseline Channel Geometry Domain as Simulated**
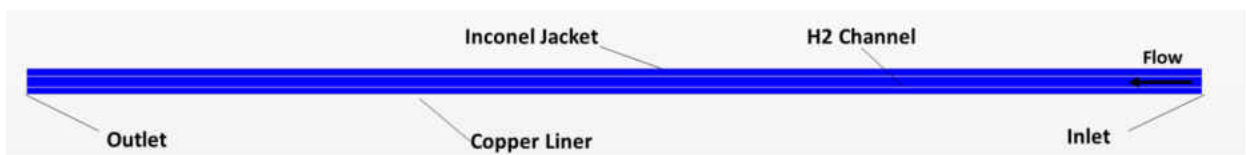


**Figure 18: Baseline Channel Geometry Side View**
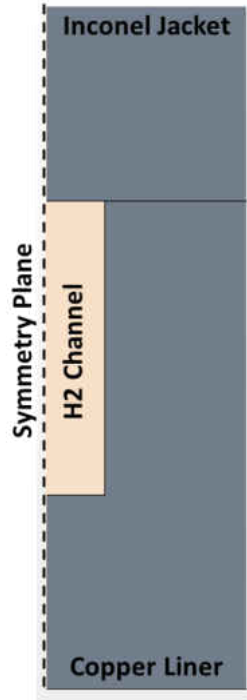
**Figure 19: Baseline Channel Geometry Front View**

The boundary conditions for the baseline case are made to emulate the baseline case from

Wadel et al [12]. The boundary conditions for all following cases will be the same as for the

baseline case, save for the hot gas wall. In the baseline case the hot gas wall has a temperature

profile imposed on it, and all following cases have a heat flux imposed on it. However, the

boundary locations are the same for all cases. The baseline boundaries can be seen in figure 20.

The symmetry plane is represented as such. The interior walls of the channel are no-slip surfaces,

and the exterior walls are adiabatic. The inlet has a mass flow rate imposed on it, and the outlet is

held at a constant pressure
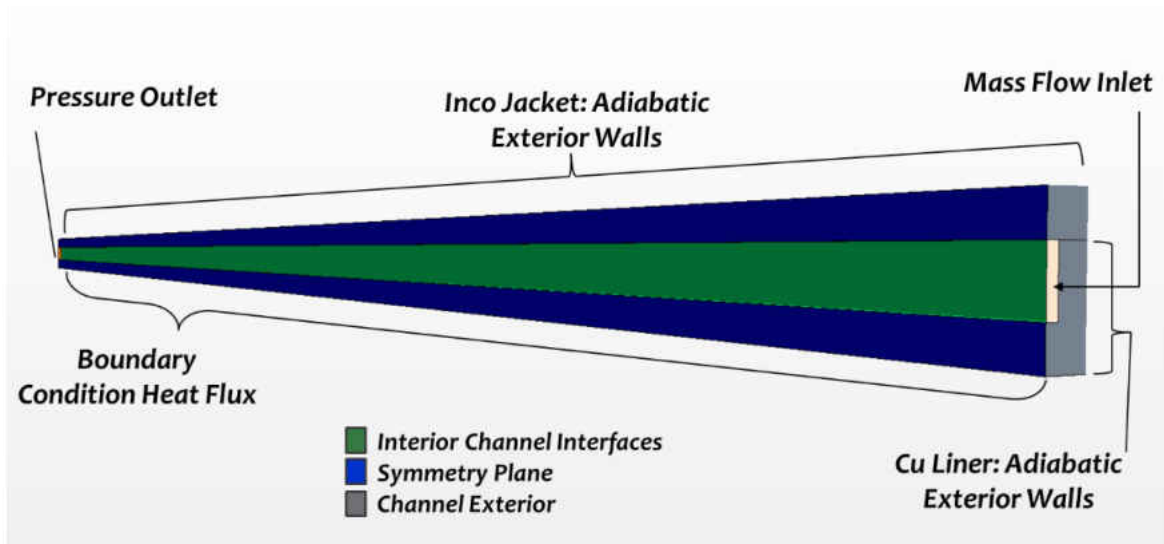
**Figure 20: Baseline Case Boundary Conditions**

## 4.2 Meshing and Assumptions

A quality mesh is important for accurate simulations and results. All cases were meshed and using STAR-CCM+ meshing tool. Due to the simple rectangular shape of the baseline channel, a structured, trimmed, mesh was considered at first. This would work well with the baseline geometry, but later cases with more complex geometry would not work will with a structured mesh. To ensure the same mesh can be used for each case, a polyhedral mesh was used instead of a trimmed mesh. Also, polyhedral cells resolve recirculation better than tetrahedral cells, and require fewer cells [20]. Prism layers were also used on walls which have a no-slip boundary condition. This is to resolve the hydrodynamic boundary layer. The Advancing Layer Prism Mesher was used to build the prism layers. This method builds the prisms from the wall outward and has less prism cell collapsing in corners.

Developing the appropriate mesh takes several iterations. There are key metrics that affect the quality of the mesh. These include the skewness angle, the y+ value, and the base

cell size. The base cell size determines the size of the cells in the mesh volume, unless a different local parameter is input, such as a prim layer near a wall, or a zone of refinement. Info into more mesh parameters can be found in the Star User Guide, under Mesh Metrics [22].

The skewness angle of a cell is the difference between the perpendicular vector on the face of the cell and the line connecting the centroids of the cells. Higher angles can cause divergence. It is desirable for the skewness angle of a mesh to be less than ninety degrees.

The y+ value is one of great importance. The flow through the channel in the current study yields a very high Reynolds number, on the order of millions. This ensures that the flow is turbulent [9]. In turbulent flows, the velocity profile near the wall is largely influenced by the y+ value. This is because a region exists that is not suitable for modeling purposes. This region, referred to as the buffer layer lays between y+ values of 5 to 30. The log-law region exists above the buffer region at y+ values of 30 to 200. The region below the buffer layer is called the viscous sublayer, which exists at y+ values of less than 5. The buffer layer is not suitable for modeling because the log of the wall does not resolve velocity accurately in this region.

$$y^+ = \frac{y}{\nu}\sqrt{\frac{\tau_w}{\rho}} \ \ or \ \ y^+ = \frac{y\mu_\tau}{\nu} \tag{14}$$

The channel Reynolds number is very high and correspondingly has high velocity. The y+ parameter is indirectly affected by velocity, equation (14). It is a function of shear stress, and higher velocities increase the shear stress. In the equation, y is the distance from the wall, $\nu$ is the kinematic viscosity, $\tau_w$ is the wall shear stress, $\rho$ is the fluid density, and $\mu_\tau$ is the shear velocity. In order to drive down the y+ value in the model prism layers are used near

the wall. Prism layers allow for extra refinement in the near wall region. In the model a total of 40 prism layers are applied to the interior walls of the fluid domain, with a growth rate of 1.2, and a total prism layer height of 1.03e-4 m, or 0.103 mm. A plot with the channel cross-sectional velocity profile can be seen in the appendix. This shows the smooth transition of the velocity from very near the wall, through the prism layers, and into the core. The y+ values can be seen on the baseline model in figure 21. The channel walls are shown from 15 to 20 cm from the inlet, where the y+ values are the highest. With y+ less than one all over the baseline channel, the y+ value should remain favorable later when features are added.
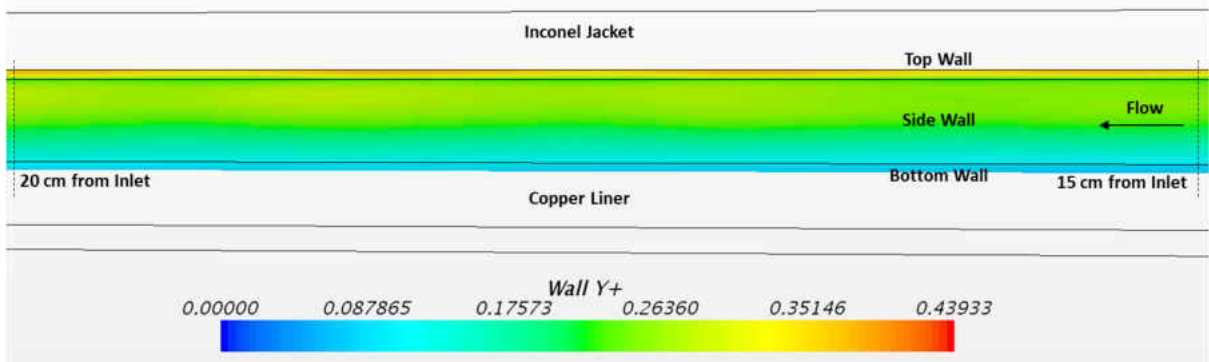


**Figure 21: Baseline Channel y+ Values for Mesh 1, Zoned in to Highest Values**

The base cell size was determined from a grid convergence investigation. Along with the chamber wall heatload convergence, as seen in figure 22, an uncertainty analysis was performed to assist in determining the proper cell size. Heatload (Q), into hot gas wall, difference between 27.6 and 31.1 million cells is 0.04%

38
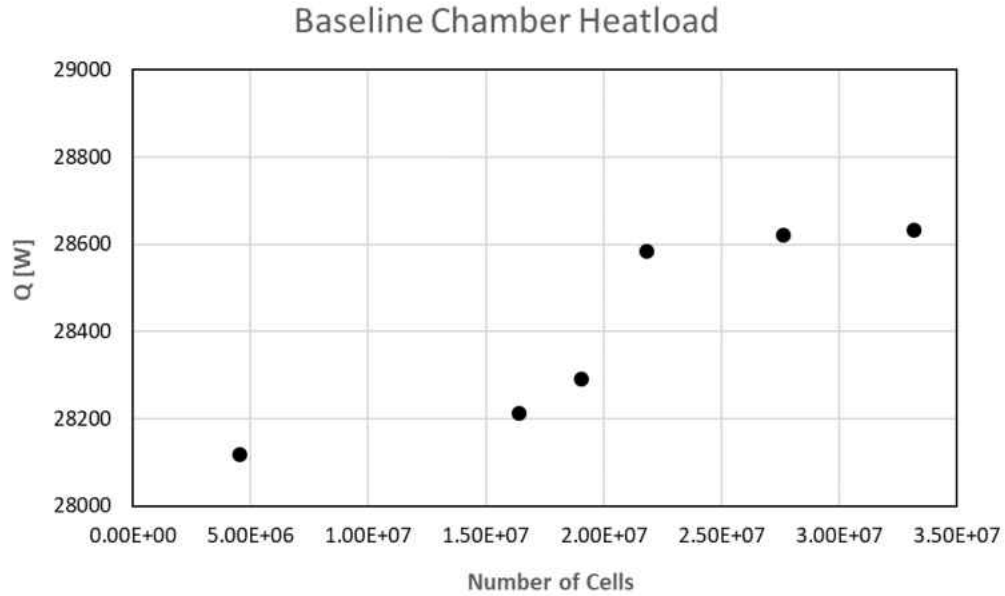
**Figure 22: Baseline Case Pressure Drop Convergence**

The method used for the uncertainty analysis is that as described by Celik et al [22]. The method entails using at least three different mesh sizes to compare key parameters to each other for the various mesh sizes. The mesh sizes used for the gird convergence investigation for the current study can be seen in table 3. The three meshes from the grid convergence investigation can be seen in the appendix. Mesh case one is the mesh that is used for the baseline simulation.

**Table 3: List of Mesh Sizes in Grid Convergence Investigation**

|        | Volume Cell Count |
|--------|-------------------|
| Mesh 1 | 27612336          |
| Mesh 2 | 16395027          |
| Mesh 3 | 1482731           |

All boundary conditions for the grid convergence investigation are the same as they would be for a normal simulation which is run for the purpose of obtaining results. The results from the grid convergence investigation can be seen in table 4.

**Table 4: Grid Convergence Investigation Results for Baseline Case**

|  | Mesh 3 | Mesh 2 | Mesh 1 | $e_a^{32}$(%) | $e_a^{21}$(%) | $GCI_{fine}^{21}$ | Extrapolated Value | $e_{ext}^{21}$(%) |
|---|---|---|---|---|---|---|---|---|
| dP | 2.103 | 2.211 | 2.291 | 0.051 | 0.035 | 0.176 | 2.613 | 0.522 |
| $\bar{T}_{out}$ | 221.2 | 215.6 | 219.6 | 0.025 | 0.018 | 0.090 | 235.4 | 0.995 |
| q" | 2.89E+04 | 2.82E+04 | 2.86E+04 | 0.024 | 0.014 | 0.071 | 3.03E+04 | 1.000 |
| $\bar{V}_{out}$ | 459.7 | 449.2 | 454.7 | 0.023 | 0.012 | 0.061 | 476.8 | 0.997 |

With the model being run using computational fluid dynamics (CFD), physics conditions need to be established. The physics models and parameters are listed below:

**For Fluid Region:**

- Steady State

- 3D

- Reynolds Averaged Navier-Stokes (RANS)

- Coupled Energy

- Coupled Flow (2nd Order)

- Gas: H2

- Ideal Gas

- Realizable K-Epsilon Turbulence (2nd Order), Two Layer

**For Solid Regions:**

- Steady State

- 3D

- Constant Density

- Coupled Solid Energy

The hydrogen in the model is in supercritical form. This means that the fluid exceeds the supercritical temperature and supercritical pressure. For hydrogen those are 1.3 MPa and 33 K, respectively. The inlet temperature of 44.4 K and outlet pressure of 11MPa means that at the minimum temperatures and pressures of the channel, the fluid is still in the supercritical region. It gets further away from the limits as it travels through the channel. Near the critical limits, fluid properties can change greatly, but as you move away from the critical limits, a supercritical fluid behaves like an ideal gas. Figure 23 shows a T-S diagram [23] for hydrogen showing that the flow stays in the critical regime the entire time it is in the channel.
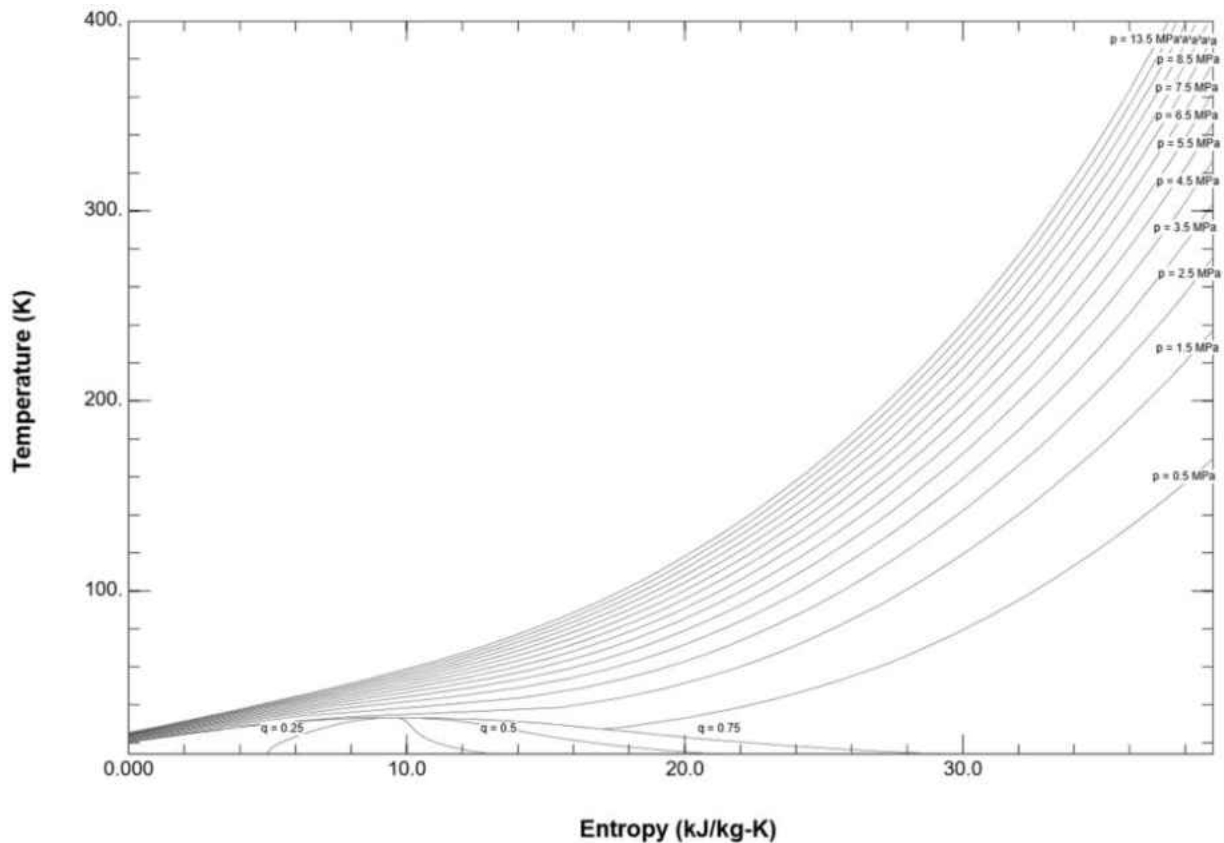


**Figure 23: T-S Diagram for Hydrogen [23]**

**Table 5: Entire Baseline Channel Dimensions**

| Geometric Parameter | Full Channel | Computational Domain |
|---|---|---|
| Channel Height [mm] | 3.18 | 3.18 |
| Channel Width [mm] | 1.27 | 0.64 |
| Aspect Ratio | 2.50 | 2.50 |
| Copper Liner Thickness [mm] | 2.10 | 2.10 |
| Inco Jacket Thickness [mm] | 2.10 | 2.10 |
| Sidewall Thickness[mm] | 1.52 | 1.52 |
| Total Width [mm] | 4.32 | 2.16 |
| Total Height [mm] | 7.37 | 7.37 |

The boundary conditions established for the baseline condition were made to emulate the environment from the baseline study in Wadel's [12] investigation. Dimensions of the whole baseline channel from the current study can be seen in table 5. Half of one channel is represented by the computational domain. With that, the inlet mass flow rate is keep at a constant 0.0115 kg/s. The outlet pressure is kept at 11 MPa, as this represents the chamber pressure from the Wadel [12] study. The exterior walls are adiabatic, while the midplane of each region is defined as a symmetry plane. The hot gas wall temperature profile from Wadel's [12] baseline study, figure 24, is applied to the hot gas side wall in the current studies model. Table 6 lists a summary of baseline case boundary conditions.

## Hot Wall Temp vs Axial Position
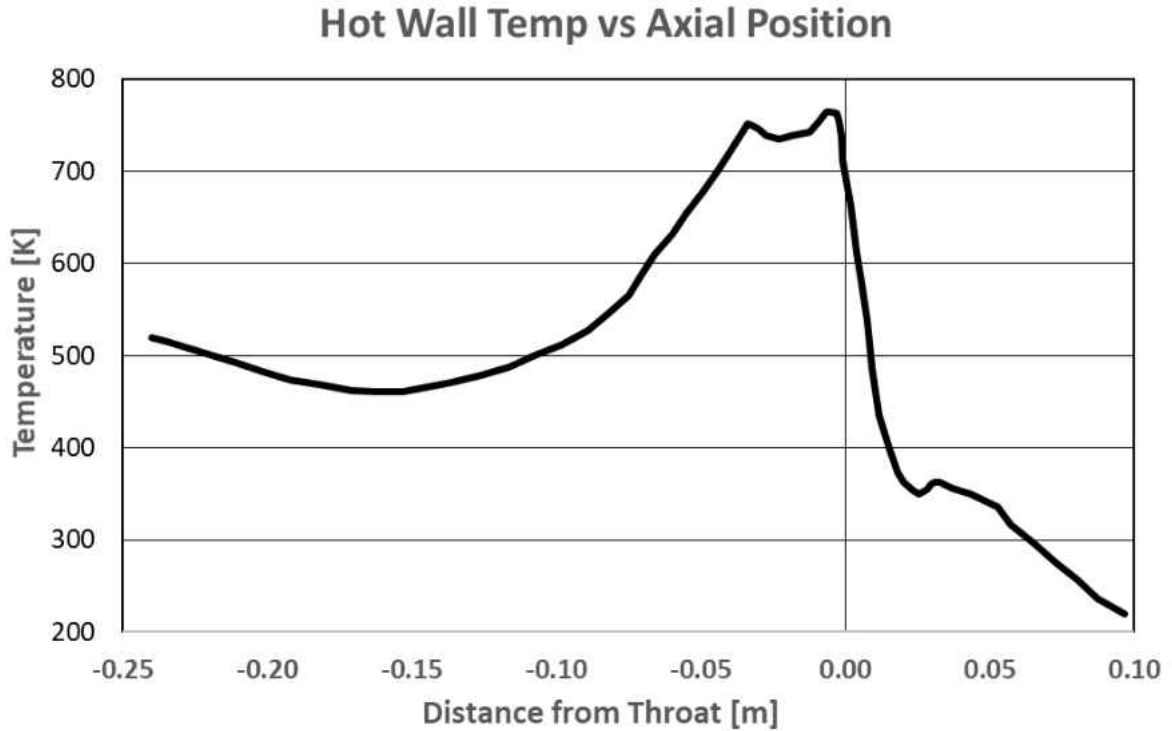


**Figure 24: Baseline Case Hot Gas Wall Temperature Profile**

**Table 6: Baseline Case Boundary Conditions**

| | |
|---|---|
| Inlet Re Number | 1.12E+06 |
| Total ṁ (100 channels)  [kg/s] | 2.2 |
| ½ Channel ṁ [kg/s] | 0.0115 |
| Uniform Inlet Temperature [K] | 44.4 |
| Outlet Pressure [MPa] | 11.0 |
| Midplane condition | Symmetry |
| Outer Wall Condition | Adiabatic |

## 4.3 Baseline Results

With the baseline analysis complete, results can be reviewed. The main goal of running the baseline was to build and establish a quality mesh, determine a hot gas wall heat flux that can be set as a boundary condition for the following cases, and to compare results from the following cases. The pressure drop for the baseline case was found to be 2.29 MPa. The maximum hot gas wall temperature (as applied) is 765 K. The heat flux going through the hot gas wall for the baseline case can be seen in figure 25. Other results from the baseline case will be shown later as a means to compare the following cases.
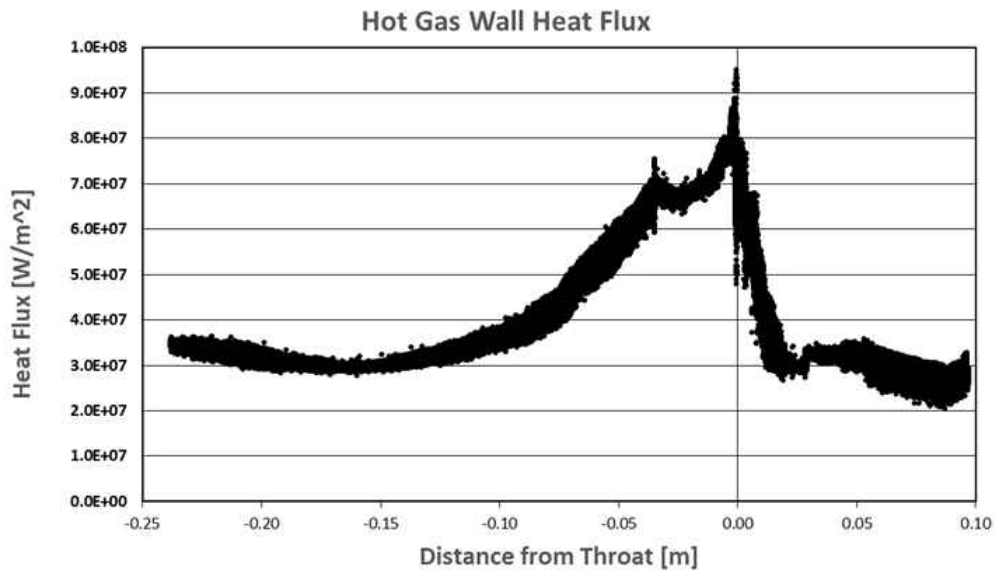


**Figure 25: Baseline Case Hot Gas Wall Heat Flux**

# CHAPTER 5: ANALYSIS OF RIBBED TURBULATOR CASE

## 5.1 Ribbed Case Geometry and Domain

The focus of the current study is to test the feasibility of using turbulators in LRE cooling channels. The intention was to do the primary analysis using wedged turbulators, as they are believed to be more efficient than ribbed turbulators. However, much research has been done on the topic of ribbed turbulators. For comparison purposes, a ribbed turbulator analysis if carried out in the current study.

For both the ribbed case and the initial wedge case, the turbulators will not be place in the entire channel. They will be place only in the near throat area where the heat flux is greatest and the hot gas wall temperature is also the largest. The goal of the current investigation is to reduce the hot gas wall maximum temperature. By placing turbulators only in the near throat area, the benefits of increased mixing near the hottest part of the channel can be gained while minimizing the pressure losses from the turbulators themselves. The near throat area is made to be from -4.89 cm from the throat location to 2.97 cm from the throat location.

The geometry for the ribbed turbulator is influenced by Han's [16] research on efficient ribbed turbulator designs. In the current study, a sixty-degree broken V rib design is utilized, as seen in figure 11. The channel with the rib feature can be seen in figure 26. A more detailed image of the ribbed feature can be seen in figure 27 showing the top-down view of the channel bottom wall, and figure 28 showing the side view from the midplane.
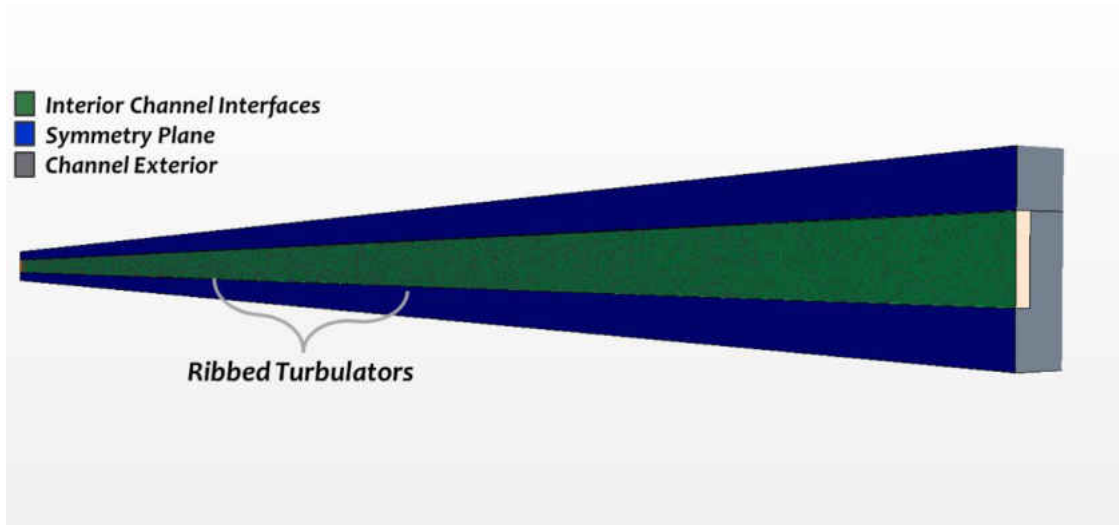
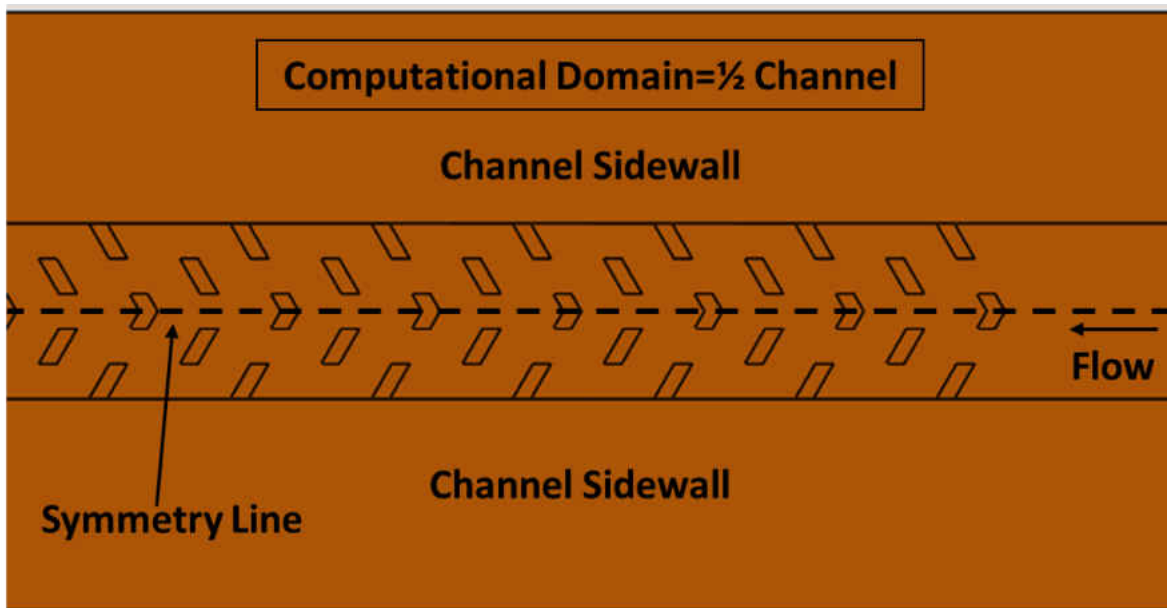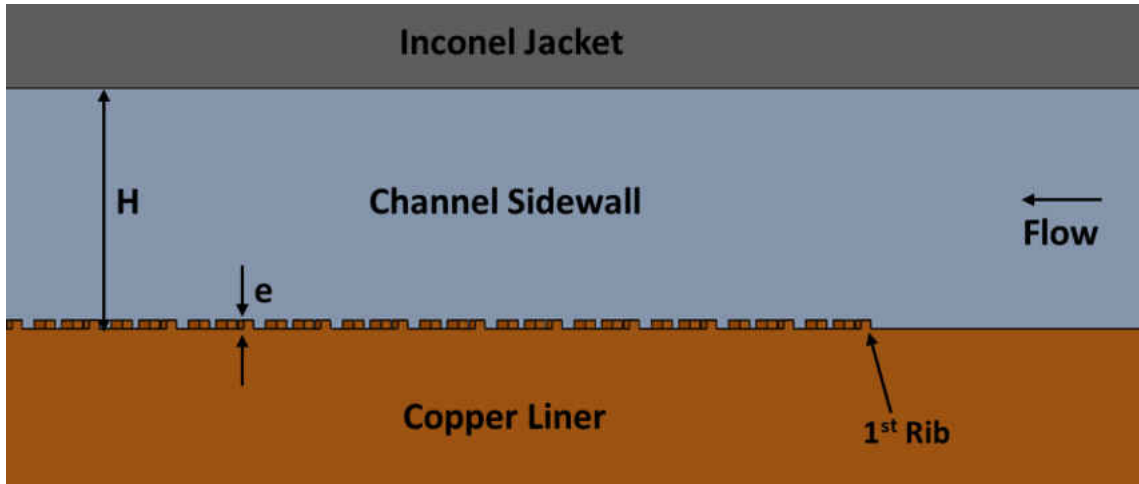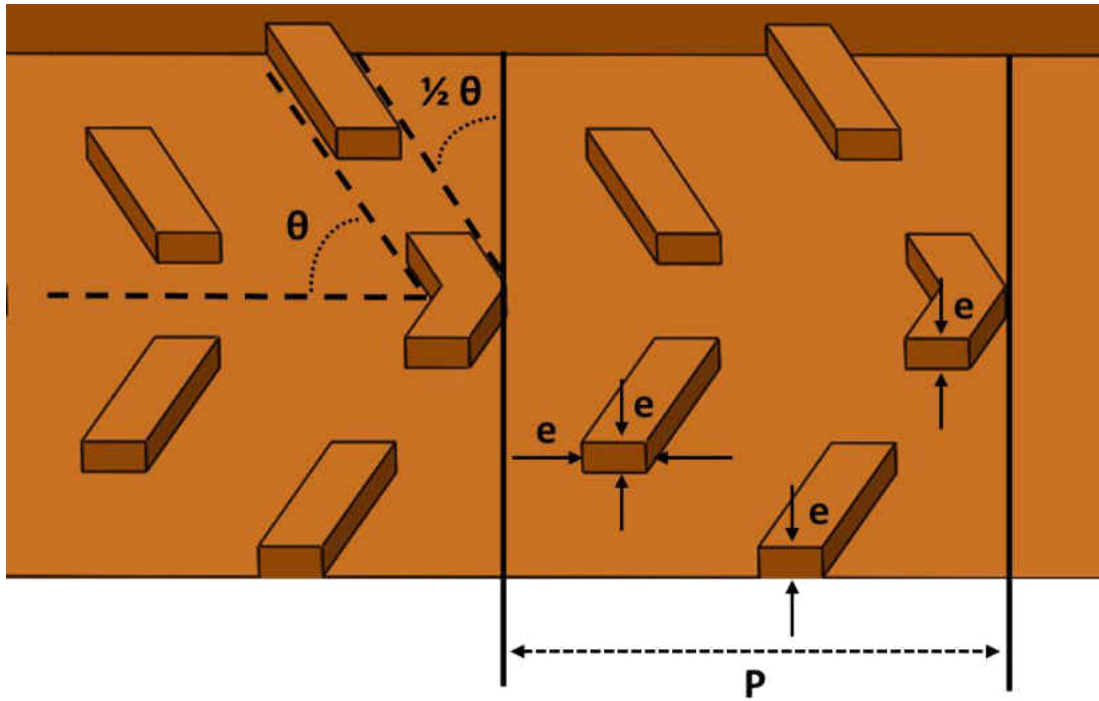**Figure 26: Ribbed Case Channel Geometry**



**Figure 27: Ribbed Case Top Down View (top wall removed)**

**Figure 28: Ribbed Case Side View from Midplane**

The rib parameters from Han [16] are used as much as they can be applied. All the ribs are square with a rib height to hydraulic diameter ratio (e/D.h) is 0.0625, and a rib height to pitch ratio of 10. The detailed geometry can be seen in figure 29.

**Figure 29: Ribbed Case Detailed Geometry**

5.2 Meshing and Boundary Conditions

Meshing of the ribbed case was done using the same base parameters as the baseline case. The region near the ribs however, on the channel bottom wall, has been refined so that the recirculation, separation, and boundary layer disruption can be accurately resolved. The core of the ribbed channel uses a base cell size of 6e-5, the same as the baseline case, but the refined region near the featured wall uses a base cell size of 5.5e-5. Further refinement of the core and the near rib area was tested. Those tests showed no appreciable difference in results. Figure 30 shows the max hot gas wall temperature convergence. The max temperature difference between the 31.9 and 35.1 million cell meshes is 0.13%. Figure 31 shows the region of highest y+ values in the domain, which still lie below 1.
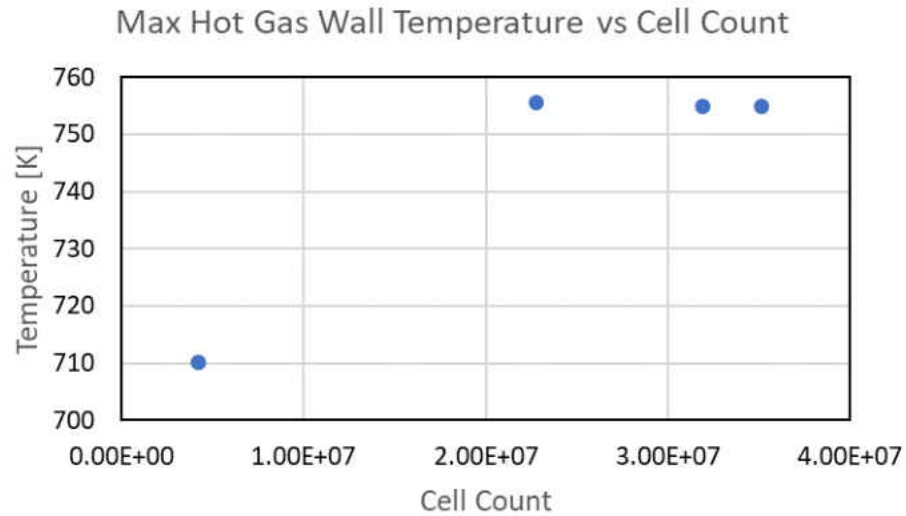
**Figure 30: Max Hot Gas Wall Temperature Convergence**
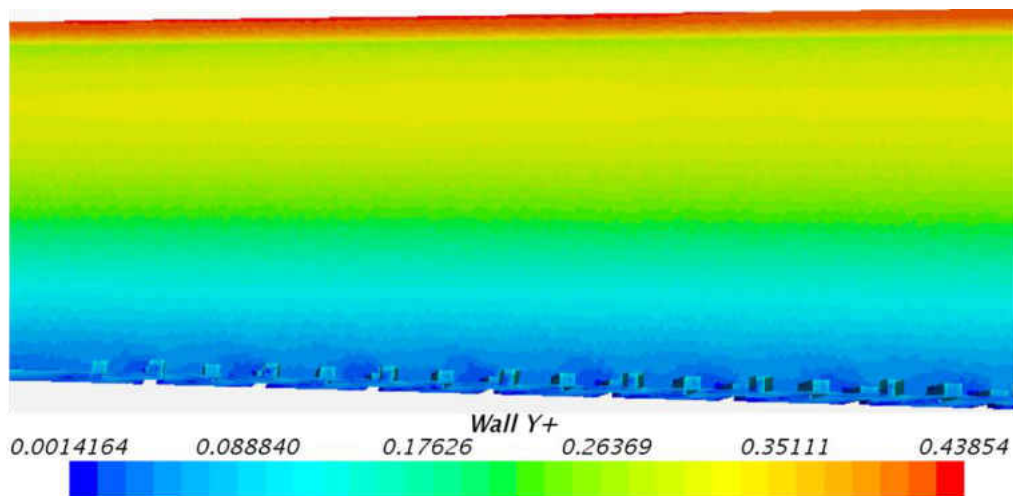


**Figure 31: Max y+ values for ribbed case mesh**

The addition of features on the channel bottom wall affects the mesh. Figure 32 shows the mesh from 0.05 mm away from the midplane side view (to show refinement zone). Another image of the prism layer near the ribs is available in the appendix. Note that from the side view one set of ribs from each pitch can be seen due to the broken configuration.
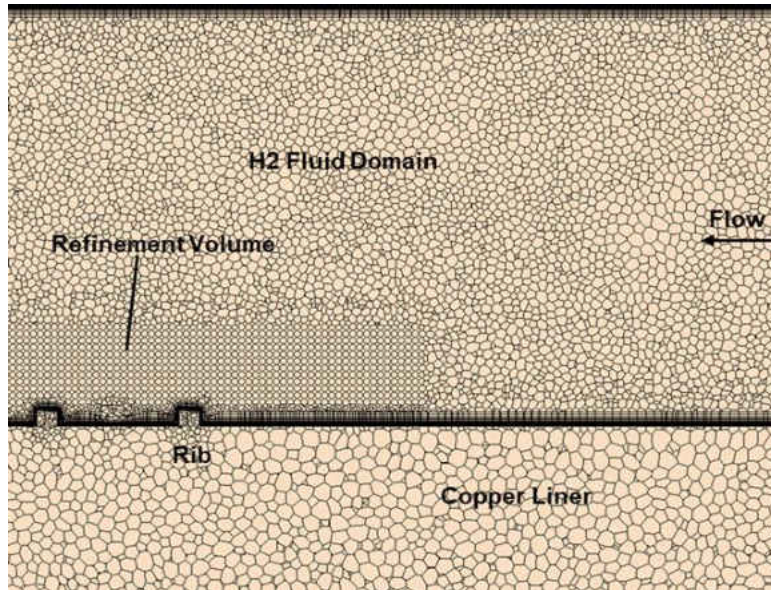
**Figure 32: Rib Case Mesh Midplane Side View**

The boundary conditions for the ribbed case are the same as in the baseline case, save for the hot gas wall. The hot gas wall for the ribbed case has a heat flux applied to it which was derived from the baseline case.

5.3 Ribbed Case Results

To investigate the feasibility of using turbulators in LRE cooling channels, the main result of interest is the hot gas side wall temperatures. These can be seen in figure 33, where they are compared against the baseline condition. Hot channel wall (bottom channel) temperatures are also included, as the reduction in the hot channel wall (or bottom channel wall) temperatures is what drives the reduction in the hot gas wall temperatures.

It is found that the hot gas wall maximum temperature from the rib case is 755 K. This represents a reduction of only 10 K when compared to the baseline results. The pressure drop through the channel of the rib case was 2.83 MPa. This is a 23.7% increase in pressure drop over

the baseline case. This could imply that using ribs in LRE cooling channels are likely not feasible, as the slight reduction in hot gas wall temperatures is at a large pressure drop penalty.

A potential reason for the ineffectiveness of the ribbed geometry in the channel is its effect of causing a step change in the oncoming flow. The flow which hits the leading edge of the rib is forced to greatly reduce its velocity, due to the rib obstruction, and move largely over the rib and also around the rib. Ninety-degree ribs have the effect of causing recirculation zones just downstream of the trailing edge of the rib, from the core fluid which is reattaching to the wall. This effect is reduced with the sixty-degree broken V rib configuration; however, the square rib still appears to cause a great loss of pressure.
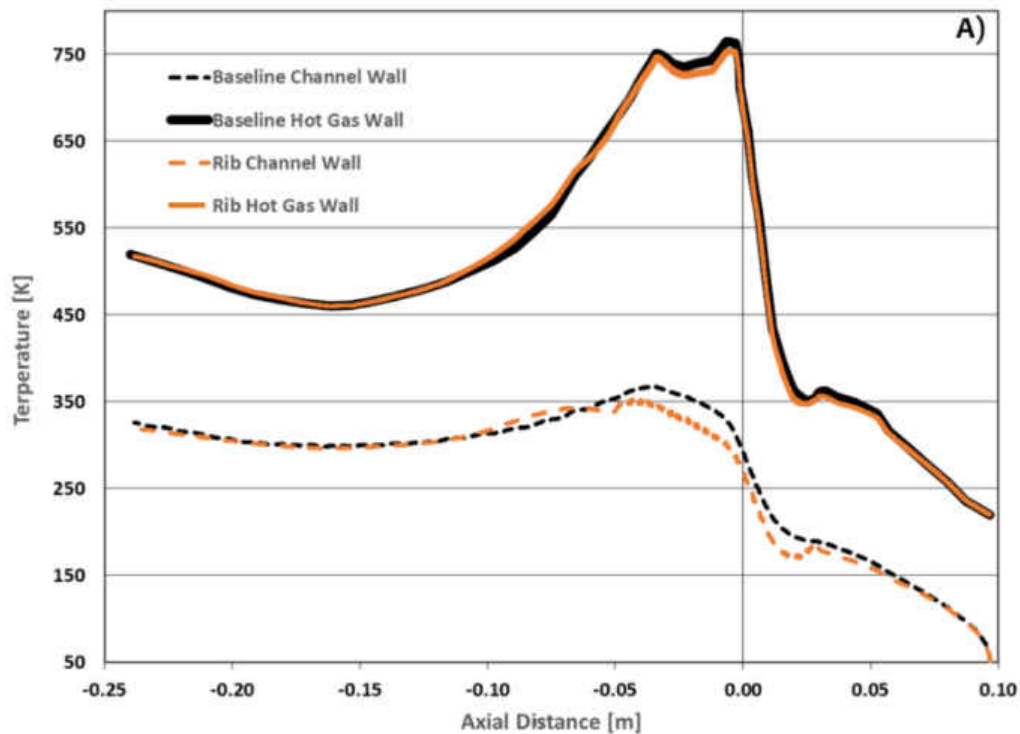


**Figure 33: Hot Gas Wall and Hot Channel Wall Temperature Profiles of Rib Case and Baseline Case**

The sixty-degree broken V ribs, to the authors' knowledge, have not been tested at such high Reynolds numbers as was modeled in the current study, at about 1.1 million. This high Reynolds number also corresponds to a high velocity. With high Reynolds number and high velocity flow, the ribs may present an obstacle that cannot be traversed thoroughly by the flow, as its stream wise momentum is too great. Figure 34 shows temperature and velocity overlaid on streamlines from the midplane side view of the first 4 pitches of ribs, which because of the staggered broken V shape, corresponds to 8 ribs. A zone of recirculation exists just downstream of the trailing edge of the ribs. This effect contributes to the lack of mixing and the lack of a substantial hot gas wall temperature reduction, due to lack of mixing.
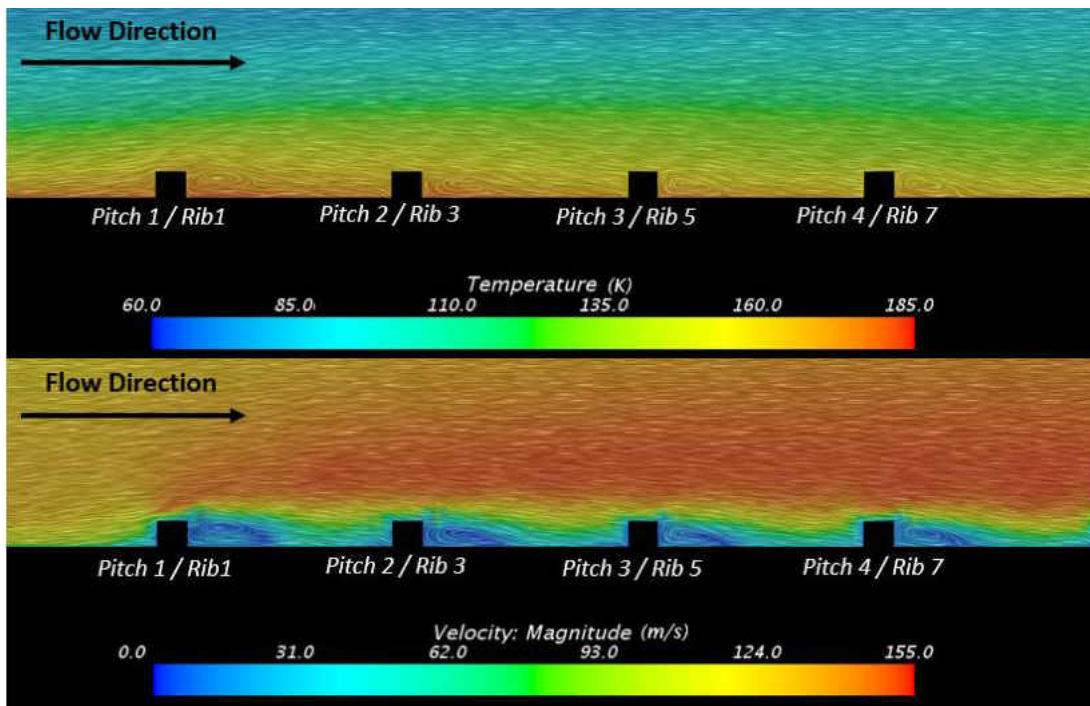


**Figure 34: Line Integral Convolution Generated Streamlines Along Channel Midplane with A) Velocity Magnitude and B) Temperature Results Shown for Ribbed Case. Side View**

From the overall channel perspective, the ribs do not efficiently mix the flow. The heat transfer coefficient through the channel of the rib case compared to the baseline case can be seen in figure 35.
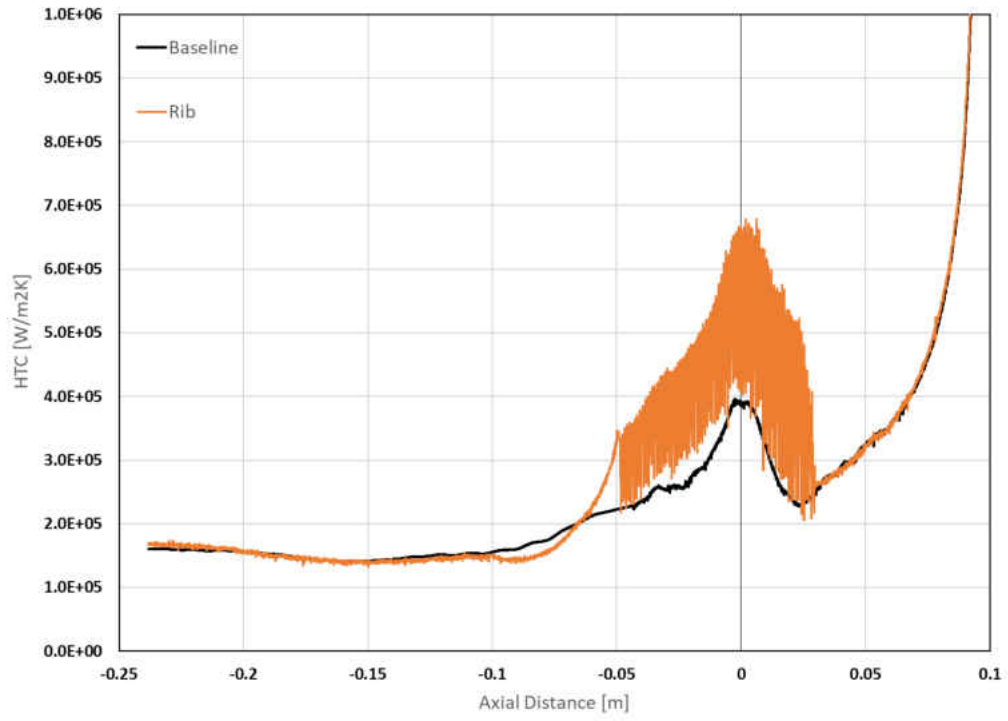
**Figure 35: Midplane Channel Bottom Wall HTC from Rib Case and Baseline Case**

# CHAPTER 6: ANALYSIS OF WEDGE TURBULATORS

## 6.1 Initial Wedge Geometry and Domain

The focus of the current study is to test the feasibility of using turbulators in LRE cooling channels. Ribbed turbulators were analyzed for reference, but backward facing delta wedges were the turbulator of greater interest. In this section the initial wedge case is discussed, then in the following section, a multiple wedge configuration analysis is discussed. The purpose of starting with an initial wedge geometry is to serve as a starting point for later comparison and to start with a geometry that is believed to be of high thermal hydraulic performance.

The geometry for the initial wedge case turbulator is obtained largely from Valentino's [18] research, who used a single larger wedge in a channel as opposed to multiple smaller ones. The initial wedge case turbulators are backward facing delta wedges, with a rib height to hydraulic diameter ratio (e/D.h) is 0.1, as per [18], a wedge angle of sixty degrees, as per [16] and a rib height to pitch ratio of 8.85. Detailed geometry can be seen in figure 36.  The channel with the initial wedge feature can be seen in figure 37. A more detailed image of the initial wedge feature can be seen in figure 38 showing the top-down view of the channel bottom wall, and figure 39 showing the side view from the midplane.
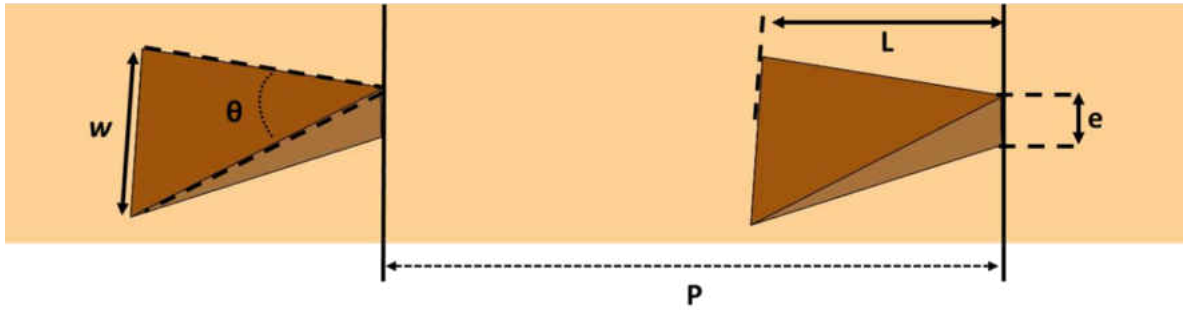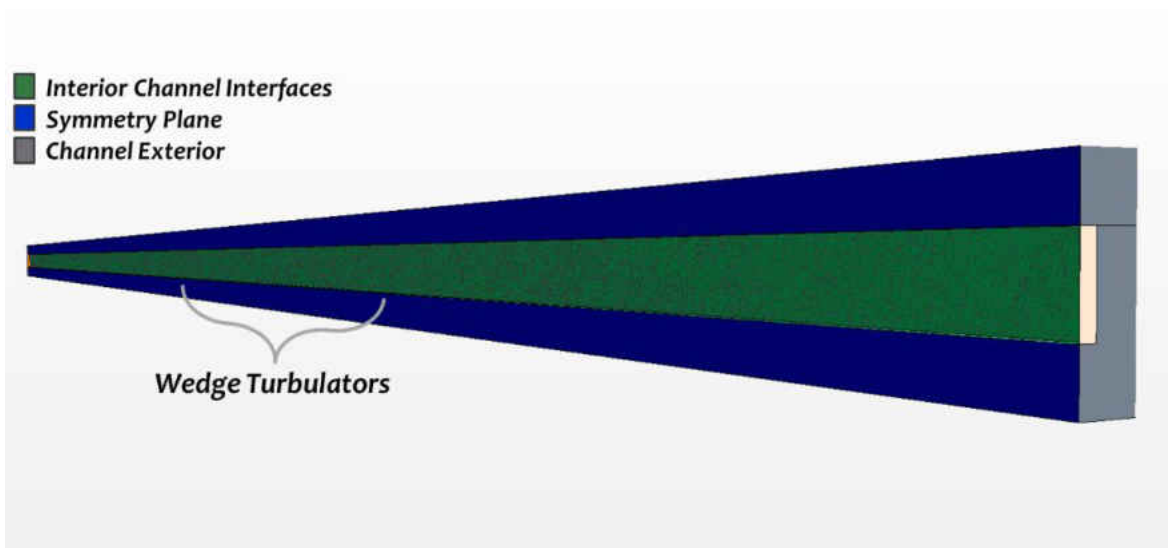
**Figure 36: Initial Wedge Case Detailed Geometry**

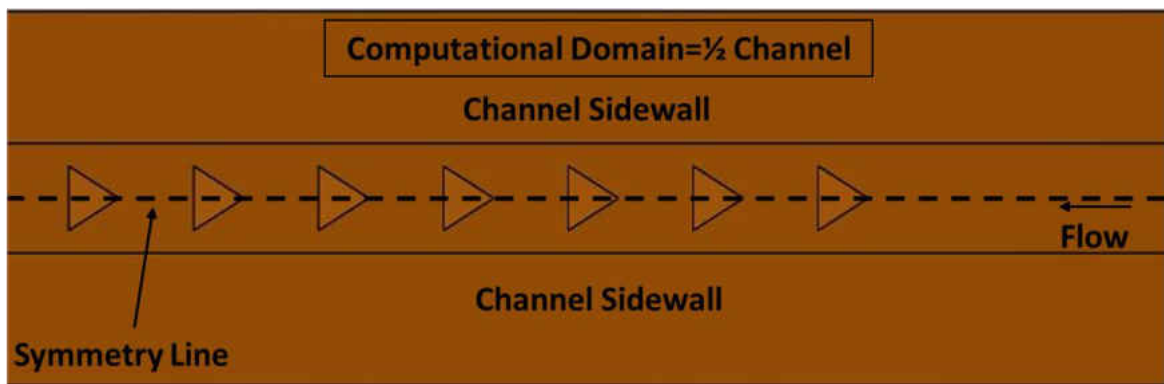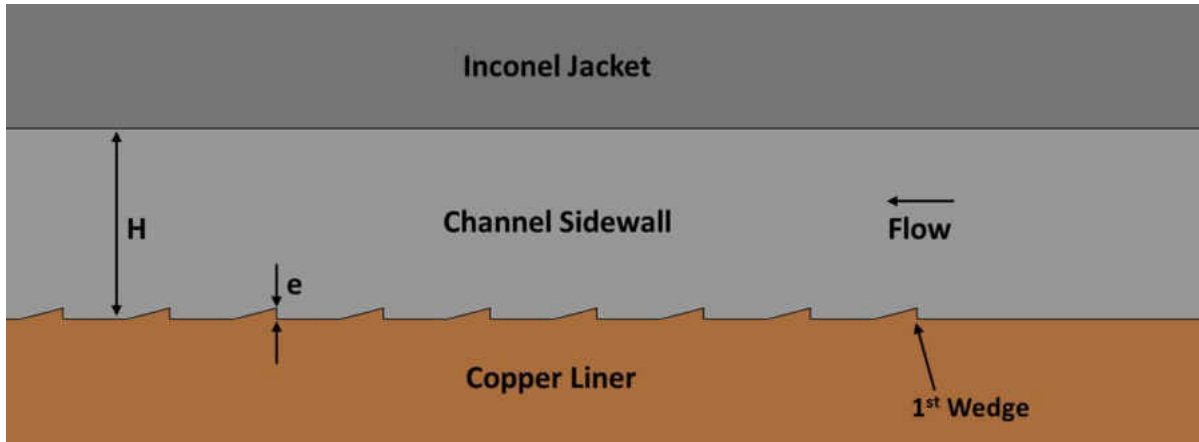

**Figure 37: Initial Wedge Case Channel Geometry**



**Figure 38: Initial Wedge Case Top Down View (top wall removed)**

**Figure 39: Initial Wedge Case Side View from Midplane**

6.2 Meshing and Boundary Conditions

Meshing of the initial wedge case was done using the same base parameters as the baseline case and rib case. The region near the wedges however, on the channel bottom wall, has been refined so that the recirculation, separation, and boundary layer disruption can be accurately resolved. The core of the ribbed channel uses a base cell size of 6e-5, the same as the baseline case, but the refined region near the featured wall uses a base cell size of 5.5e-5. Further refinement of the core and the near rib area was tested. Those tests showed no appreciable difference in results.

The addition of features on the channel bottom wall affects the mesh. Figure 42 shows the mesh from the midplane side view. A view of the initial wedge case mesh closer to the prism layers can be found in the appendix. Figure 40 shows the max hot gas wall temperature

convergence. The max temperature difference between the 29.5 and 31 million cell meshes is

0.08%. Figure 41 shows the region of highest y+ values in the domain, which still lie below 1.5.
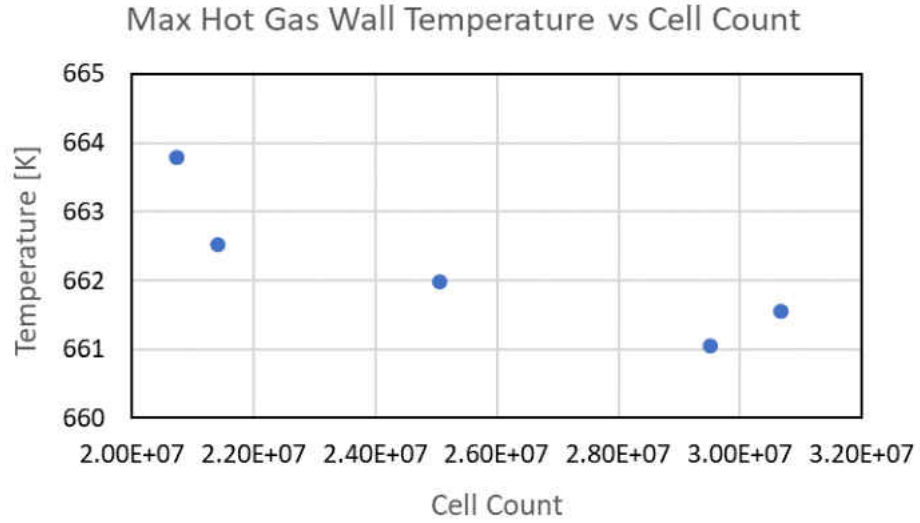


**Figure 40: Max Hot Gas Wall Temperature Convergence**
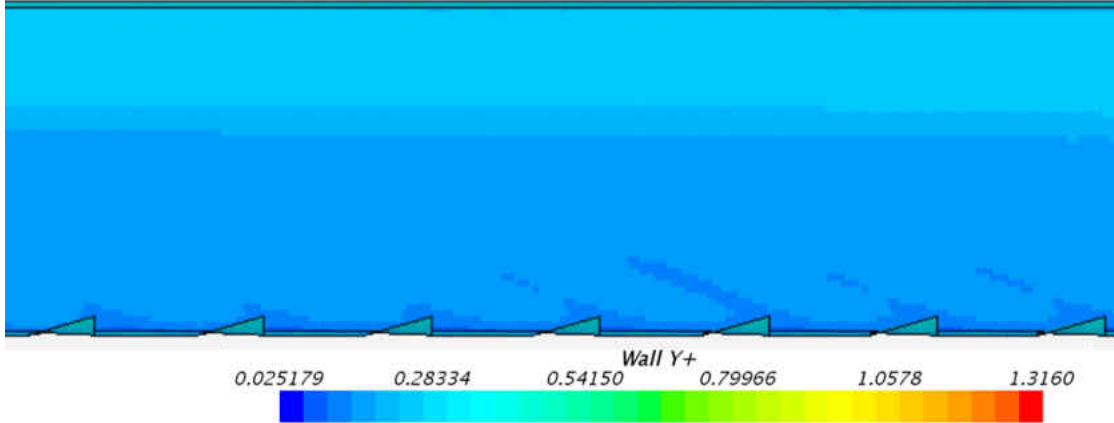


**Figure 41: Max y+ Values for Initial Wedge Case Mesh**

**Figure 42: Initial Wedge Case Mesh Midplane Side View**

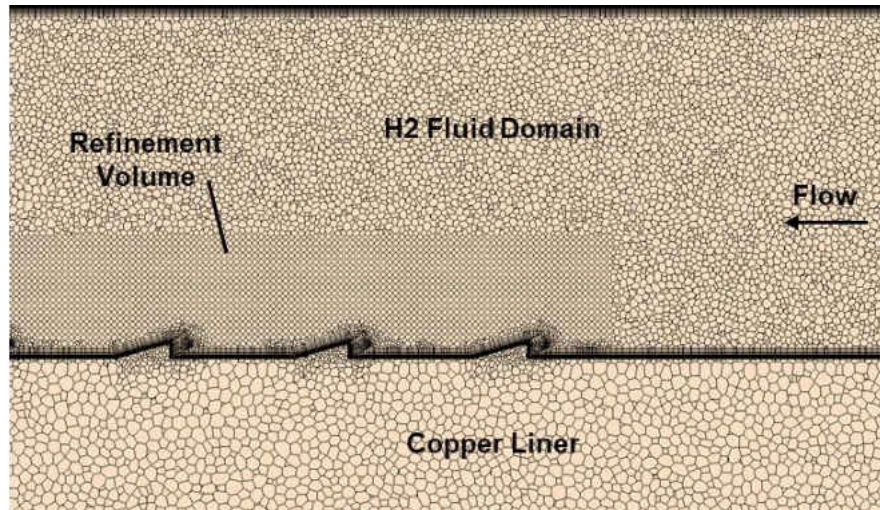The boundary conditions for the initial wedge case are the same as in the baseline case and rib case, save for the hot gas wall. The hot gas wall for the initial wedge case, like the rib case, has a heat flux applied to it which was derived from the baseline case.

## 6.3 Initial Wedge Results

The main result of interest is the hot gas side wall temperatures, to study the feasibility of using wedges in LRE cooling channels. These can be seen in figure 43, where they are compared against the baseline condition. Hot channel wall (bottom channel wall) temperatures are also included, as mentioned before, the reduction in the hot channel wall (or bottom channel wall) temperatures is what drives the reduction in the hot gas wall temperatures.

It is found that the hot gas wall maximum temperature from the initial wedge case is 661 K. This represents a reduction of 104 K when compared to the baseline results. The pressure

drop through the channel of the initial wedge case was 2.58 MPa. This is a 12.4% increase in

pressure drop over the baseline case. This implies that using the initial wedge geometry in LRE

cooling channels are more feasible than sixty-degree broken V shaped ribs, as used in the rib

case. The hot gas wall temperature has been reduced over ten times more than the ribbed case,

and the pressure increase (as a percentage of original pressure drop) is about half of what it is in

the ribbed case.
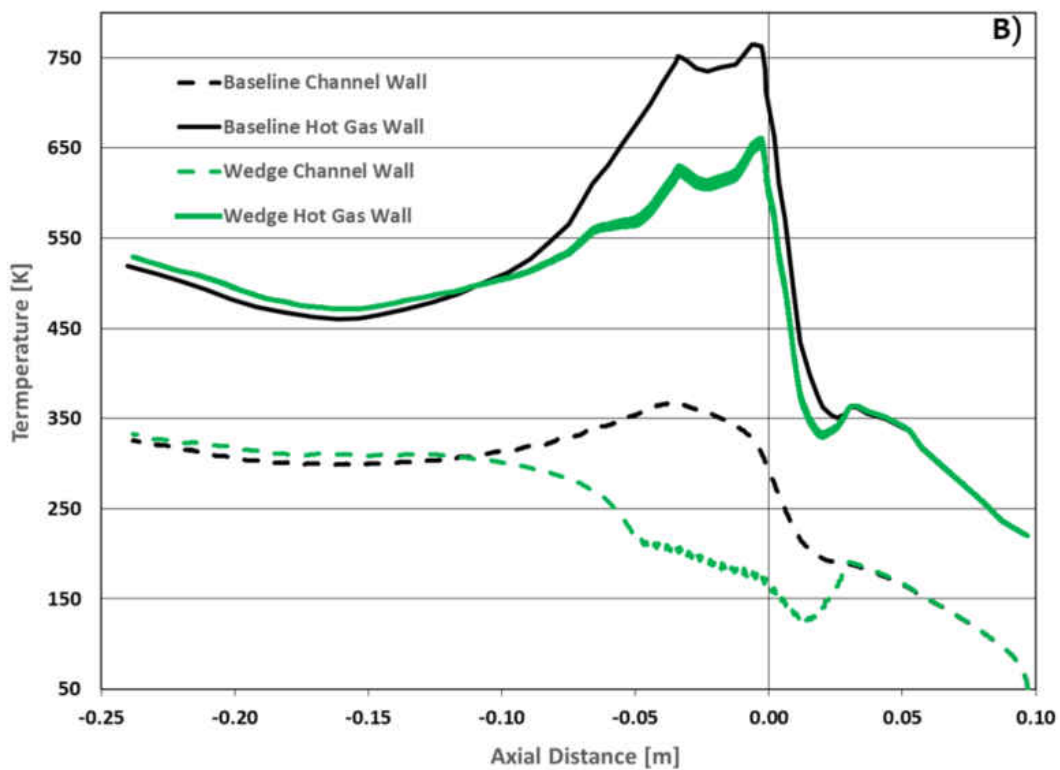


**Figure 43: Hot Gas Wall and Hot Channel Wall Temperature Profiles of Initial Wedge Case and Baseline Case**

A potential reason for the effectiveness of the initial wedge geometry in the channel is

how it mixes. A backward facing wedge does more efficiently what a ribbed turbulator intends to

do. For instance, the square rib directs flow laterally around it, but it also directs flow directly

over it which, which increase pressure losses. The backward facing delta wedge on the other

hand, serves to separate the flow laterally, while forcing very little fluid to abruptly change direction by moving completely over the wedge. This lateral separation of the oncoming flow turns into vortices which rotate largely normal to the stream wise direction, which means it can increase mixing on the featured surface and maintain its stream wise momentum much better than the ribbed case. When these vortices are created near the surface, due to the conservation of angular momentum, mirrored vortices are created alongside them closer to the core, which further increases mixing. There are also secondary vortices which occur when the flow reaches the end of the wedge near the channel wall surface and begin to rotate due to the lower pressure fluid traveling down the backward face of the wedge. Vortices are also created as the flow passes the edge wall of the wedge and mixes with the lower pressure fluid traveling down the backward face of the wedge. The mentioned vortices can be seen in figure 44. This axially rotating (swirling) motion is more efficient for mixing the flow than rib induced rotation which creates recirculation zones. The swirling of the fluid mixes the fluid from the hot wall nearer the core.
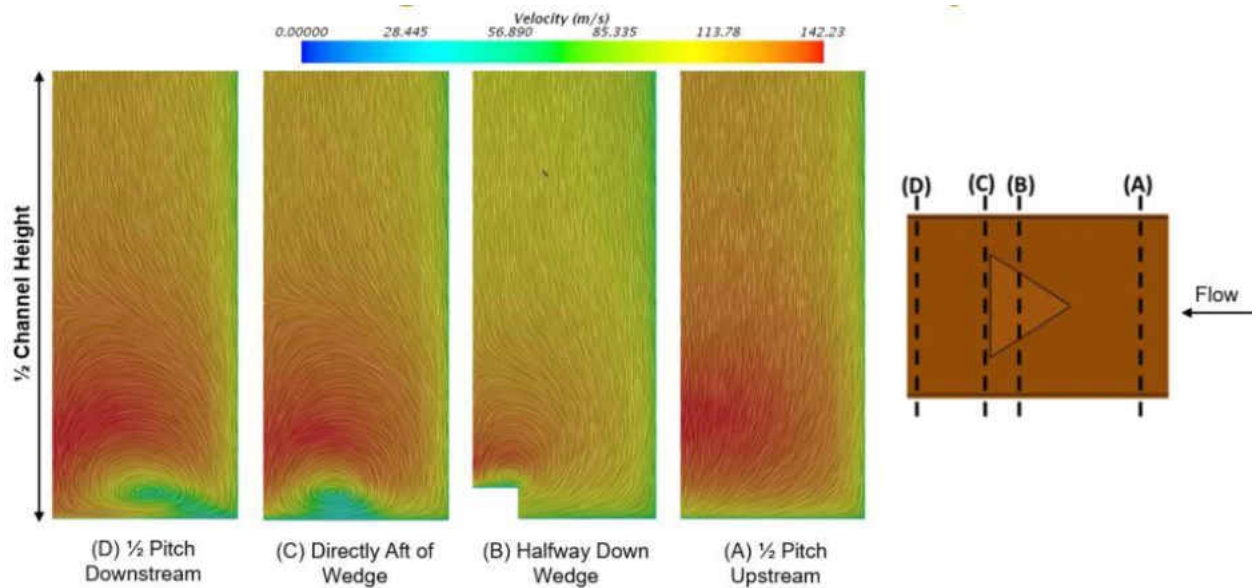


**Figure 44: Initial Wedge Case Line Integral Convolution with Velocity Magnitude Shown Along the First Wedge in the Axial Direction**

The initial wedge case geometry, to the authors knowledge, have not been tested at such high

Reynolds numbers as was modeled in the current study, at about 5.6 million. Wedges appear to

mix the flow better than the rib case geometry in this high Reynolds number flow. This could be

due to the method by which the wedge creates vortices as opposed to the rib case geometry, as

discussed earlier. Figure 45 shows temperature and velocity overlaid on streamlines from the

midplane side view of the first four wedges. Figure 46 shows temperature and velocity overlaid

on streamlines from the top-down view (0.07mm from surface) of the first four wedges. It can be

seen that mixing near the hot channel wall (channel bottom wall) surface is much greater than the

mixing caused by the rib case.
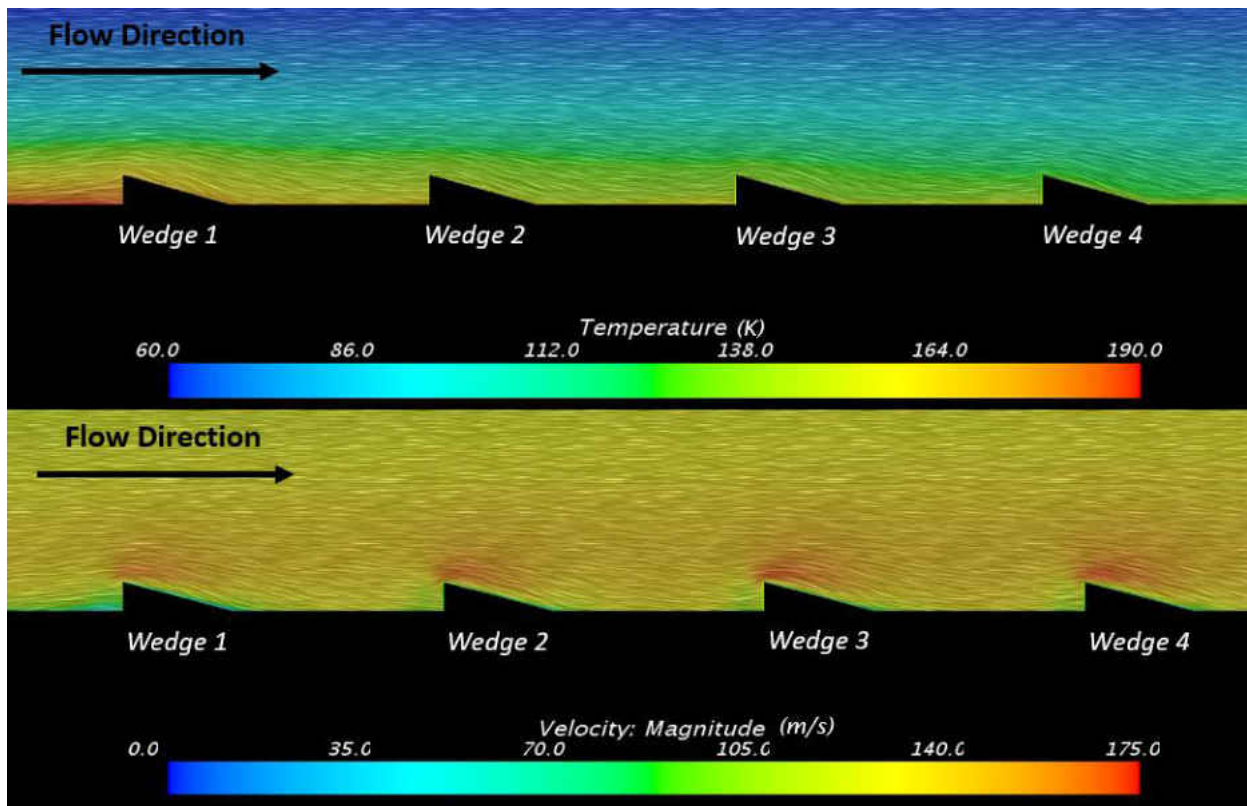


**Figure 45: Line Integral Convolution Generated Streamlines Along Channel Midplane with A) Velocity Magnitude and B) Temperature Results Shown for Initial Wedge Case. Side View**
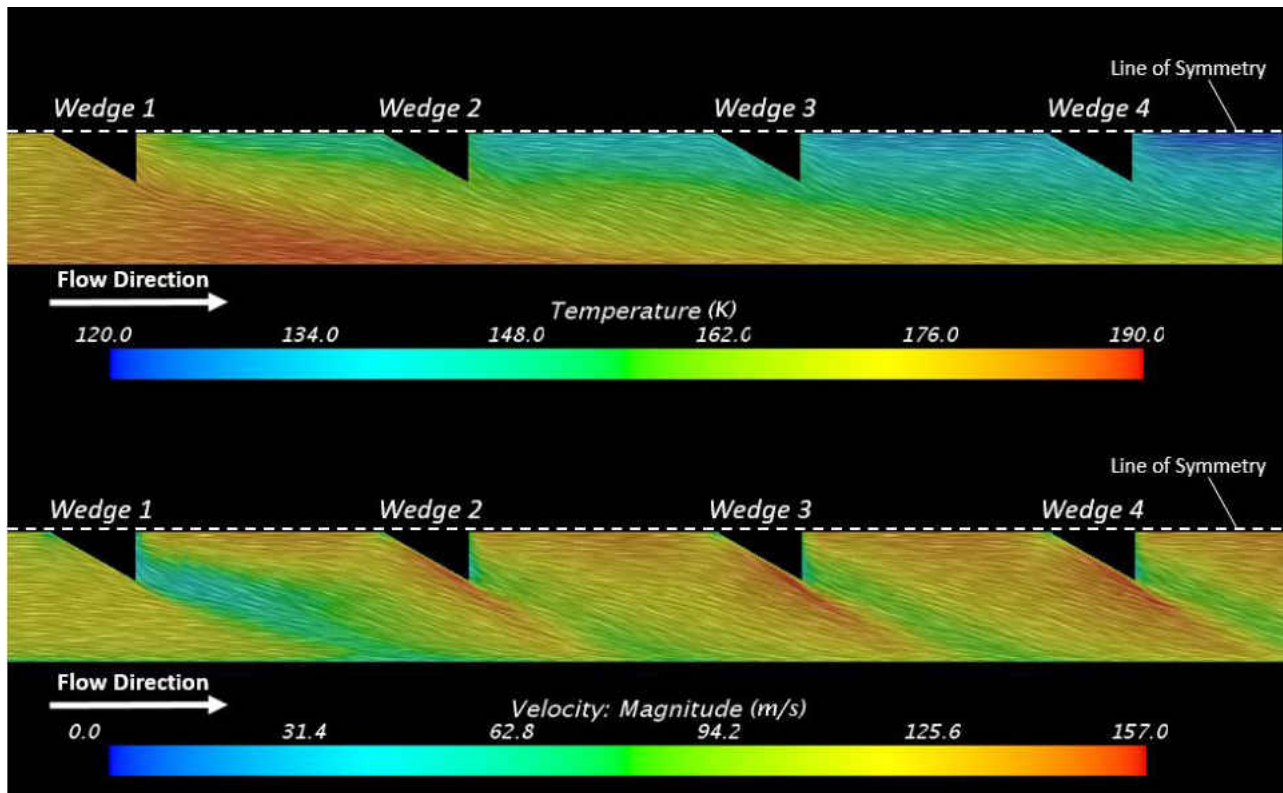
**Figure 46: Line Integral Convolution Generated Streamlines 0.07 mm above bottom channel wall with A) Velocity Magnitude and B) Temperature Results Shown for Initial Wedge Case. Top-Down View**

From the overall channel perspective, the initial wedges are much more feasible than the ribbed case. The heat transfer coefficient through the channel of the initial wedge case compared to the baseline case can be seen in figure 47. Table 7 compares the results of the initial wedge case, ribbed case, and the baseline case.
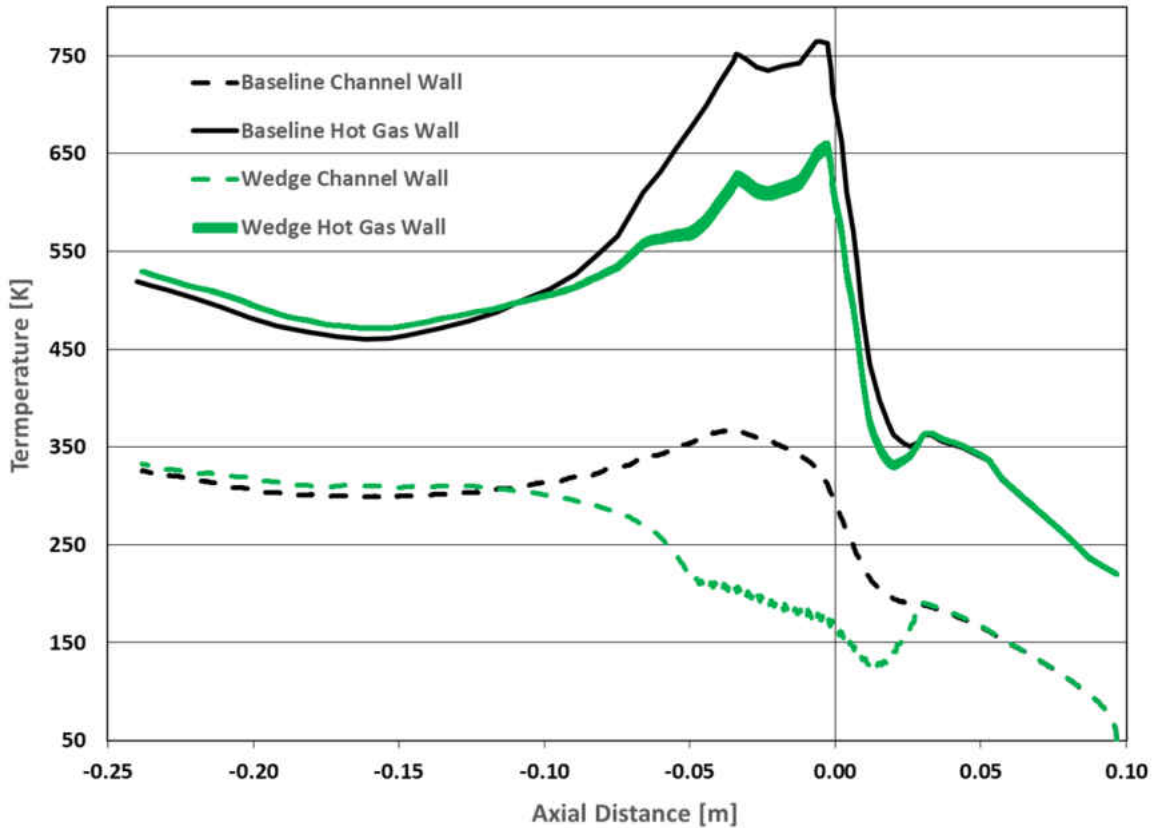
**Figure 47: Midplane Channel Bottom Wall HTC from Initial Wedge Case and Baseline Case**

**Table 7: Comparison of Results of Rib, Initial Wedge, and the Baseline Case**

| Baseline, Rib, & Initial Wedge Results | | | |
|---|---|---|---|
| Case | Baseline | Rib | Initial Wedge |
| Maximum Hot Wall Temp [K] | 765 | 755 | 661 |
| Max Temp Reduction [K] | N/A | 10 | 104 |
| Pressure Drop Through Channel [MPa] | 2.29 | 2.83 | 2.58 |
| Pressure Drop Increase [%] | N/A | 23.65 | 12.40 |

6.4 Multi-Configuration Wedge Geometry

After analyzing the initial wedge design, an analysis is conducted on numerous wedge

configurations.  Of interest in this study is how the various configurations compare against each

63

other. It reveals which wedge configuration is most efficient of those studied in the current investigation. In order to parameterize the various wedge configurations, it was determined that three factors of the wedge geometries would change, which are factors frequently studied. The wedge angle, the wedge height, and the wedge pitch changes. The angle has a great effect on mixing and how vigorously the flow is redirected toward the sidewalls. The height determines how much of the flow is pierced by the feature, which causes mixing further from the feature wall surface. The pitch has the effect of determining how periodically the flow will be tripped, thus causing more or less mixing depending on how far apart the feature are.

The initial wedge configuration was sixty degrees. In the multi wedge analysis, the wedge angles studied are twenty, fourth, sixty, and eighty degrees. The eighty degrees came from a geometric limitation of the channel, it is the largest angle that can be used without completely blocking the flow near the surface. Intervals of twenty the initial sixty lead to the forty and twenty-degree wedges.

In the initial wedge case, the wedge height is related to wedge height and the hydraulic diameter by e/D.h. For the initial wedge case that ratio is equal to 0.1. To establish bounds for the multi configuration analysis, it was determined that the wedges used will also include wedge height to hydraulic diameter ratios (e/D.h) of double (0.2) and half (0.05) of the initial wedge case's ratio of 0.1. In absolute terms that comes to a height of 0.09 mm for e/D.h of 0.05, a height of 0.18 mm for e/D.h of 0.1, and 0.36 mm for e/D.h of 0.2.

The pitch of the initial wedge case is 1.1 mm. This means that every 1.6 mm a new wedge begins. This corresponds to a total of 49 wedges in the channel, in the near throat region. Like the wedge height, it is desired to double, and halve the pitch. This however cannot be done, as if the pitch were to halve, the wedge features would interfere with each other, occupying the

same space. With this in mind, the wedge configurations studied utilized pitches that were, doubled at 3.3 mm and corresponding to 24 total wedges in the channel near throat region, and reduced to two thirds of the initial wedge pitch at 1.1 mm, which corresponds to 74 total wedges in the channel near throat region.

In total Thirty-six different configurations of a delta wedge in the present study's cooling channel were simulated. Wedge angle, wedge height, and pitch were the three parameters that were varied for the multiple configuration study. Table 8 shows the parameters that were varied and by how much.

**Table 8: Wedge Parameter Values for Multi-Configuration Study**

| Wedge Angle θ [Degrees] | 20 | 40 | 60 | 80 |
|---|---|---|---|---|
| | | | | |
| **Wedge Height e [mm]** — Absolute [mm] | 0.09 | 0.18 | 0.36 | |
| **Wedge Height e [mm]** — e/D.h | 0.05 | 0.1 | 0.2 | |
| | | | | |
| **Pitch** — Absolute [mm] | 1.06 | 1.61 | 3.28 | |
| **Pitch** — # of Wedges | 74 | 49 | 24 | |
| **Pitch** — Initial Scale | 2/3 | 1 | 2 | |
| | Length (L, fixed) = 0.64 mm | | Width (W, variable) = f(θ) | |

6.5 Multi-Configuration Wedge Results

It is desired to investigate the effects of the parameters on the thermal performance of each geometry. Figures 48 and 49 show the max hot gas wall temperature and channel pressure drop, respectively, for the multi-configuration cases with respect to their angle. The plotted

configurations colors and shapes represent; height (e/D.h) = 0.05 (blue), 0.1 (orange), 0.2 (green), and pitch (mm) = 1.06 (triangle), 1.61 (circle), 3.28 (square). The plots show that there is a large decrease in max temperature as the wedge angle is increased from 20 to 40 degrees, then the returns begin to diminish as the wedge angle is further increased. The pressure drop on the other hand seems to continue to increase as the wedge angle is increased further.
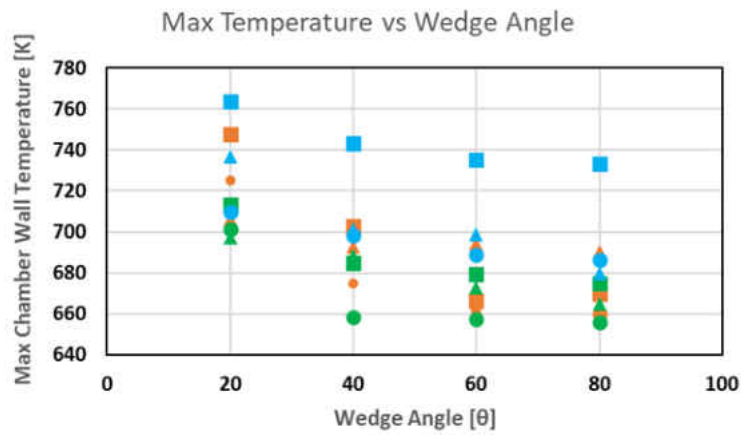


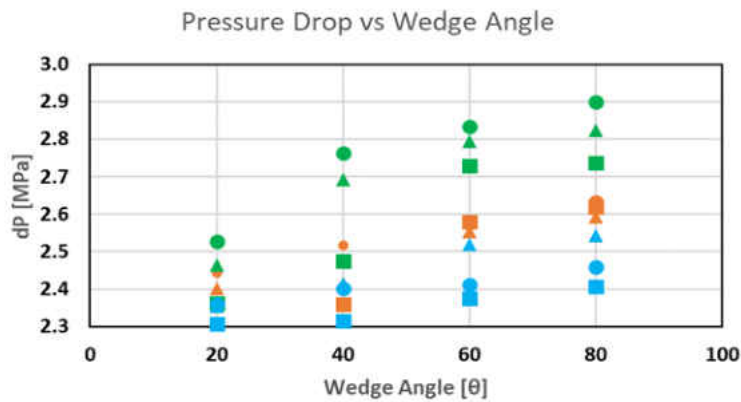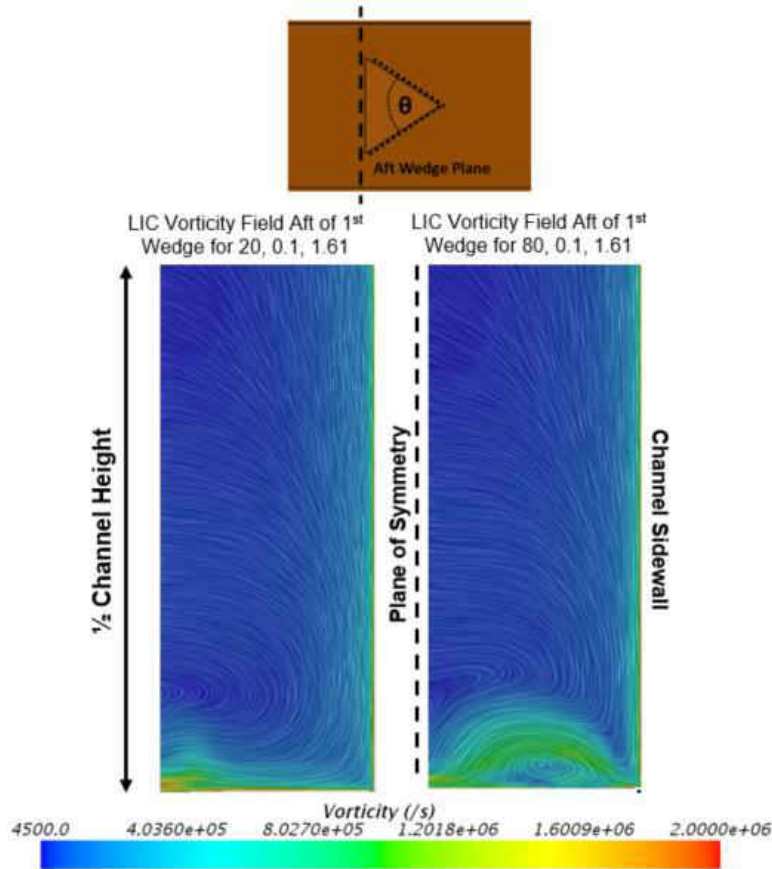**Figure 48: Max Hot Gas Wall Temperature vs Wedge Angle for Multi-Config Wedges**



**Figure 49: Channel Pressure Drop vs Wedge Angle for Multi-Config Wedges**
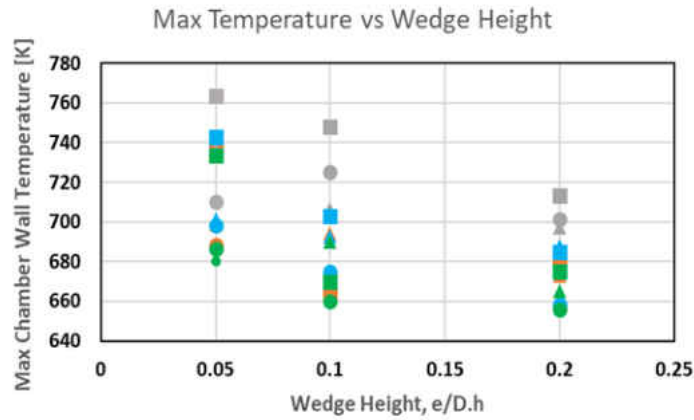
66

**Figure 50: LIC with Vorticity Magnitude Shown for 80 and 20 Degree Wedges. Directly Aft of the Wedge.**

Figure 50 shows the Line Interval Convolution plots (LIC) for 80 and 20-degree cases with a constant e/D.h of 0.1 and a constant pitch of 1.61 mm. The larger wedge angle creates vortices over a larger area of the bottom wall surface thereby improving mixing. Their larger angle increases pressure drop continually because it represents a larger obstacle for the flow to overcome.

Figures 51 and 52 show the max hot gas wall temperature and channel pressure drop, respectively, for the multi-configuration cases with respect to their height. The plotted configurations colors and shapes represent; Angle (Deg) =20 (grey), 40 (blue), 60 (orange), 80 (green), and pitch (mm) = 1.06 (triangle), 1.61 (circle), 3.28 (square). The plots show that there

is a continual decrease in max temperature as the wedge height is increased from an e/D.h value

of 0.05 to 0.2. The pressure drop also continues to raise as the wedge height increases.



**Figure 51: Max Hot Gas Wall Temperature vs Wedge Height for Multi-Config Wedges**
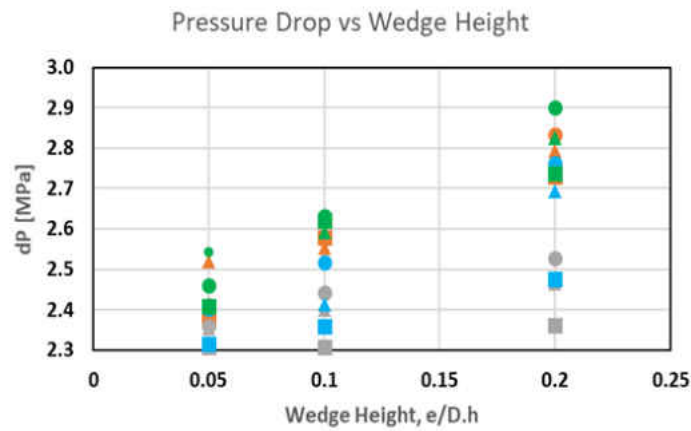


**Figure 52: Channel Pressure Drop vs Wedge Height for Multi-Config Wedges**
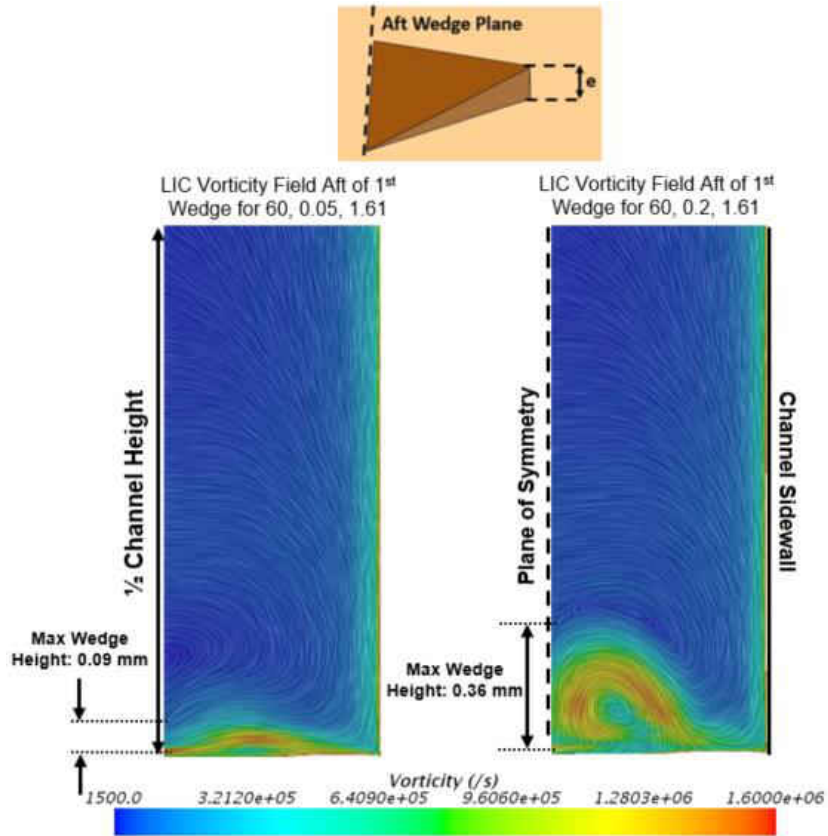
**Figure 53: LIC with Vorticity Magnitude Shown for 80 and 20 Degree Wedges. Directly Aft of the Wedge.**

Figure 53 shows the Line Interval Convolution plots (LIC) for an e/D.h value of 0.05 and 0.2, with a constant angle of 60 degrees and a constant pitch of 1.61 mm. The taller rib, by penetrating the flow more than a shorter one, serves to create a swirling effect in the fluid parallel with the flow direction that extends further from the bottom channel wall. This larger vortex created serves to increase mixing which helps lower the max hot gas wall temperature, but it also contributes to a greater pressure loss in the channel due to the increased chaos of the fluid near the bottom wall.

Figures 54 and 55 show the max hot gas wall temperature and channel pressure drop, respectively, for the multi-configuration cases with respect to their pitch. The plotted configurations colors and shapes represent; Angle (Deg) =20 (grey), 40 (blue), 60 (orange), 80

(green), and height (e/D.h) = 0.05 (triangle), 0.1 (circle), 0.2 (square). The plots show that there

is a decrease in max hot gas wall temperature as the pitch changes from 1.06 to 1.61 mm, then an

increase as the pitch increases again to 3.28. The pressure drop on average is lowest for the

largest pitch of 3.28 mm. It is similar for the 1.06 and 1.61mm pitches with exaggerated pressure

drops for the larger angle wedges.
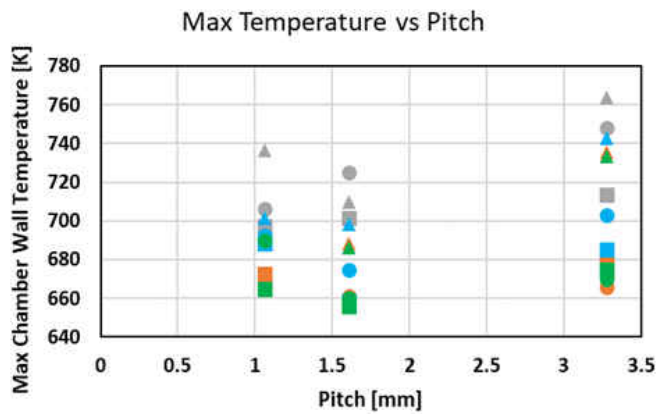


**Figure 54: Max Hot Gas Wall Temperature vs Wedge Pitch for Multi-Config Wedges**
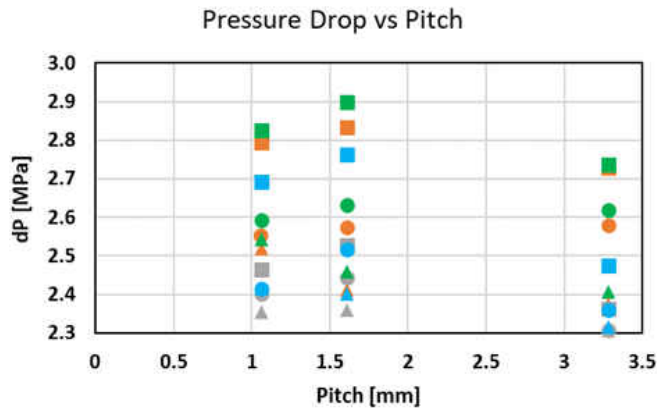


**Figure 55: Channel Pressure Drop vs Wedge Pitch for Multi-Config Wedges**
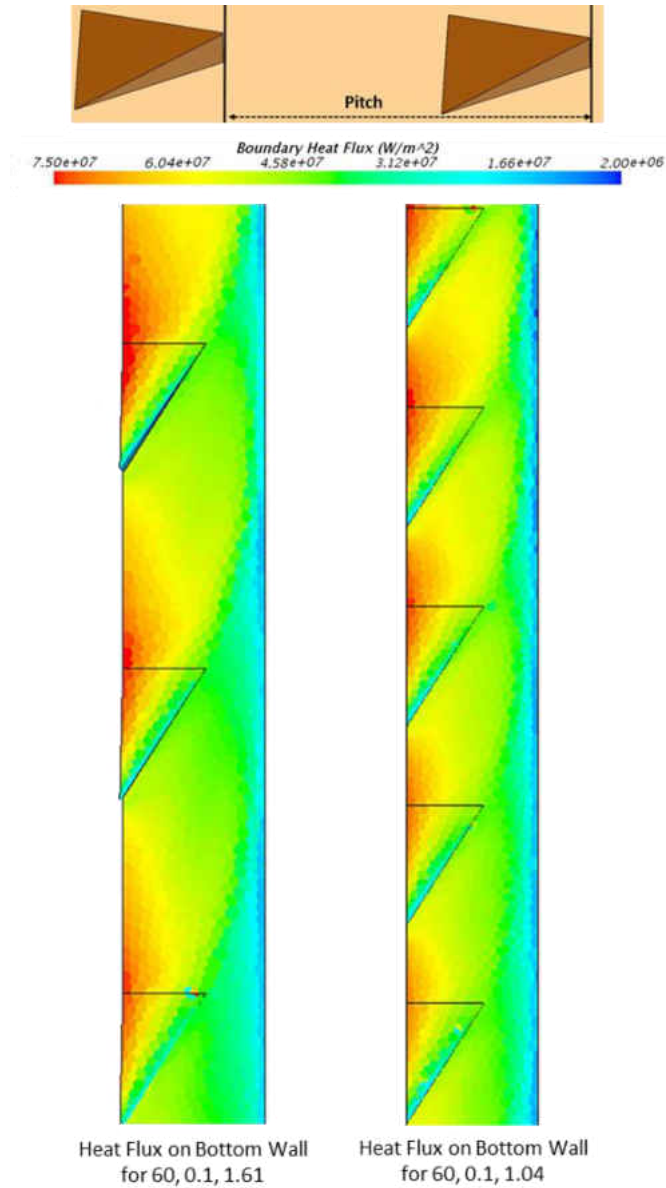
**Figure 56: Heat Flux Through Bottom Channel Wall and Wedges for Pitches of 1.61 and 1.04 mm with Constant Angle of 60 Degrees and e/D.h of 0.1**

Figure 56 shows the heat flux through the bottom channel wall and wedges. It shows that the downwash zone aft of the wedge is an area that sees increased flux. This may help reduce the max temperature of the 1.61 mm pitch configurations compared to the 1.04 mm pitch configurations by increasing the surface area on the bottom channel wall in the downwash zone where the increased heat transfer is occurring. For the largest pitch of 3.28 mm the wedges

communication between one another is much less than the lower pitch cases. The increased

pressure drop of the 1.61mm pitch configuration over the 1.04 mm pitch configuration is

exaggerated with higher angle and height wedges, and may also result from the increased bottom

wall surface area and more room for reattachment of the boundary layer, which when disrupted

again contributes to increasing pressure losses.

Table 9 shows the tabulated results of all the multi-configuration wedge cases. In the baseline

case twice as much heat traveled through the channel sidewall than the bottom channel wall. The

sidewall makes up about 70 percent of the channel surface area and the bottom wall only about

15 percent. In all other cases with wedges, the flux through the bottom wall increased and the

flux through the sidewalls decreased. This is due to the wedges increasing the HTC on the

bottom wall much more effectively than on the sidewalls. As the max hot wall temperature

decreases, the ratio of sidewall flux to bottom wall flux also decreases. Figure 57 shows the h/h.0

(channel average HTC over Baseline channel average HTC) and f/f.0 (channel friction factor

over Baseline friction factor) for all wedge cases run. The HTC and Darcy friction factor used

for this calculation can be seen in equations (15) and (16), respectively. Some configurations are

more efficient by increasing the HTC with little increase in the friction factor. The baseline

channel average HTC is 2.39e5 W/m2K and the baseline Darcy friction factor is 0.01696.

Heat Transfer Coefficient $\qquad \bar{h} = \dfrac{q_{total}}{A_{surf}(\bar{T}_{surf} - \bar{T}_{bulk})}$

(15)

Darcy Friction Factor $\qquad \Delta P_{ch} = f \dfrac{L_{ch}}{D_h} \dfrac{\rho_{avg} V_{avg}^2}{2}$

(16)

## Table 9: Tabulated Results from All Wedge Cases

| Angle Degrees | $\dfrac{e}{D_h}$ | Pitch mm | Wedges Total | $T_{max}$ K | dP MPa | $\dfrac{h}{h_0}$ | $\dfrac{f}{f_0}$ | $\dfrac{q_{sidewall}}{q_{bottom}}$ | $\dfrac{h_{sidewall}}{h_{BL\_sidewa}}$ |
|---|---|---|---|---|---|---|---|---|---|
| Baseline Case | | | | 765 | 2.29 | 1.00 | 1 | 2.08 | 1 |
| 20 | 0.1 | 1.61 | 49 | 725 | 2.44 | 1.18 | 1.06 | 1.72 | 0.98 |
| 20 | 0.1 | 3.28 | 24 | 748 | 2.31 | 1.12 | 1.01 | 1.93 | 0.99 |
| 20 | 0.1 | 1.06 | 74 | 706 | 2.40 | 1.21 | 1.02 | 1.61 | 0.95 |
| 20 | 0.2 | 1.61 | 49 | 701 | 2.53 | 1.21 | 1.11 | 1.65 | 0.97 |
| 20 | 0.2 | 3.28 | 24 | 713 | 2.36 | 1.19 | 1.05 | 1.66 | 0.96 |
| 20 | 0.2 | 1.06 | 74 | 697 | 2.47 | 1.25 | 1.10 | 1.61 | 0.96 |
| 20 | 0.05 | 1.61 | 49 | 710 | 2.36 | 1.17 | 1.02 | 1.58 | 0.92 |
| 20 | 0.05 | 3.28 | 24 | 764 | 2.31 | 1.10 | 1.00 | 1.89 | 1.00 |
| 20 | 0.05 | 1.06 | 74 | 737 | 2.35 | 1.15 | 1.01 | 1.73 | 0.97 |
| 40 | 0.1 | 1.61 | 49 | 675 | 2.52 | 1.27 | 1.07 | 1.53 | 0.92 |
| 40 | 0.1 | 3.28 | 24 | 703 | 2.36 | 1.20 | 1.02 | 1.59 | 0.93 |
| 40 | 0.1 | 1.06 | 74 | 693 | 2.41 | 1.25 | 1.08 | 1.60 | 0.95 |
| 40 | 0.2 | 1.61 | 49 | 658 | 2.76 | 1.28 | 1.19 | 1.55 | 0.93 |
| 40 | 0.2 | 3.28 | 24 | 685 | 2.48 | 1.24 | 1.06 | 1.56 | 0.92 |
| 40 | 0.2 | 1.06 | 74 | 688 | 2.69 | 1.24 | 1.20 | 1.62 | 0.95 |
| 40 | 0.05 | 1.61 | 49 | 698 | 2.40 | 1.25 | 1.06 | 1.58 | 0.94 |
| 40 | 0.05 | 3.28 | 24 | 743 | 2.32 | 1.13 | 1.01 | 1.83 | 0.98 |
| 40 | 0.05 | 1.06 | 74 | 701 | 2.41 | 1.22 | 1.03 | 1.60 | 0.95 |
| 60 | 0.1 | 1.61 | 49 | 661 | 2.58 | 1.28 | 1.10 | 1.52 | 0.91 |
| 60 | 0.1 | 3.28 | 24 | 666 | 2.58 | 1.28 | 1.12 | 1.53 | 0.93 |
| 60 | 0.1 | 1.06 | 74 | 694 | 2.55 | 1.27 | 1.17 | 1.62 | 0.95 |
| 60 | 0.2 | 1.61 | 49 | 657 | 2.83 | 1.28 | 1.24 | 1.61 | 0.93 |
| 60 | 0.2 | 3.28 | 24 | 679 | 2.73 | 1.24 | 1.19 | 1.59 | 0.94 |
| 60 | 0.2 | 1.06 | 74 | 673 | 2.79 | 1.26 | 1.27 | 1.62 | 0.94 |
| 60 | 0.05 | 1.61 | 49 | 689 | 2.41 | 1.27 | 1.06 | 1.53 | 0.93 |
| 60 | 0.05 | 3.28 | 24 | 735 | 2.38 | 1.19 | 1.08 | 1.77 | 0.98 |
| 60 | 0.05 | 1.06 | 74 | 699 | 2.52 | 1.25 | 1.12 | 1.57 | 0.95 |
| 80 | 0.1 | 1.61 | 49 | 660 | 2.63 | 1.28 | 1.14 | 1.52 | 0.91 |
| 80 | 0.1 | 3.28 | 24 | 670 | 2.62 | 1.24 | 1.20 | 1.62 | 0.97 |
| 80 | 0.1 | 1.06 | 74 | 690 | 2.59 | 1.26 | 1.17 | 1.58 | 0.95 |
| 80 | 0.2 | 1.61 | 49 | 656 | 2.90 | 1.29 | 1.29 | 1.61 | 0.93 |
| 80 | 0.2 | 3.28 | 24 | 675 | 2.74 | 1.25 | 1.23 | 1.61 | 0.96 |
| 80 | 0.2 | 1.06 | 74 | 665 | 2.82 | 1.27 | 1.29 | 1.61 | 0.96 |
| 80 | 0.05 | 1.61 | 49 | 686 | 2.46 | 1.23 | 1.08 | 1.52 | 0.93 |
| 80 | 0.05 | 3.28 | 24 | 733 | 2.41 | 1.20 | 1.10 | 1.75 | 0.97 |
| 80 | 0.05 | 1.06 | 74 | 680 | 2.54 | 1.24 | 1.13 | 1.57 | 0.95 |
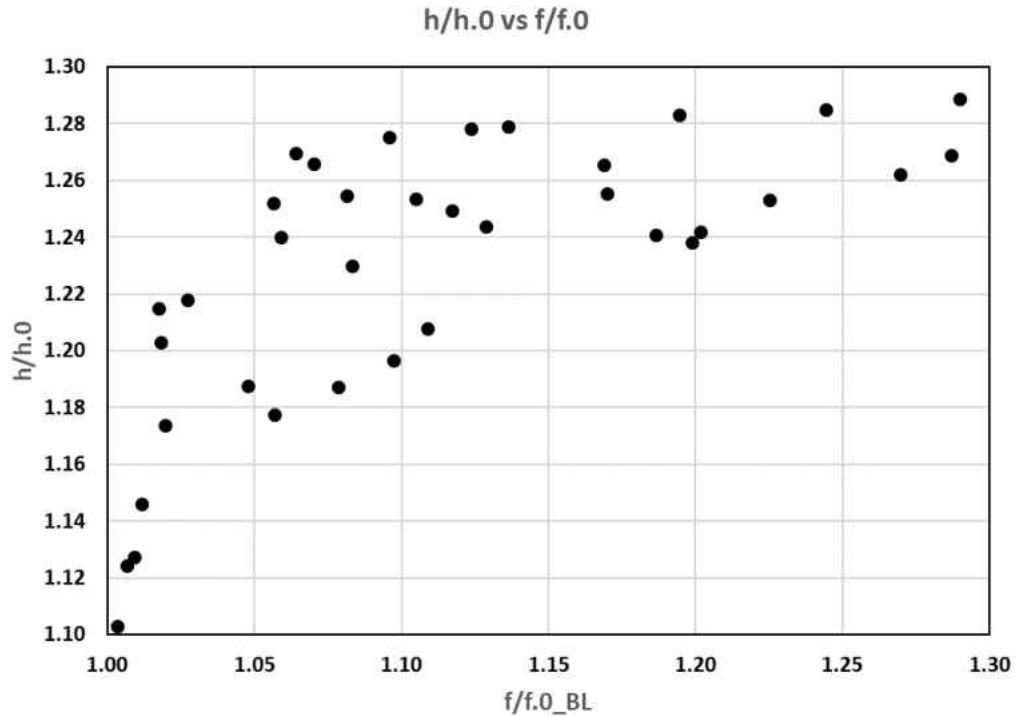
**Figure 57: h/h.0 vs f/f.0 for All Wedge Cases**

Figure 58 shows the feasibility front with all wedge cases run. It reveals what thermal performance is possible with the investigated geometries. To the left of the front is not possible to reach, and to the right is a sub-optimal area where the temperature decrease is at a greater pressure loss. The front is made of points laying closest to the x and y axis. The best tradeoff point is the point closest to the origin in the plot. Figure 59 shows the feasibility front with all wedge cases labeled. No cases with a pitch of 1.06 mm lay on the front, indicating that is not an efficient configuration. Smaller wedge angles and heights are nearer the left end of the plot while larger wedge angles and heights are nearer the right end of the plot.
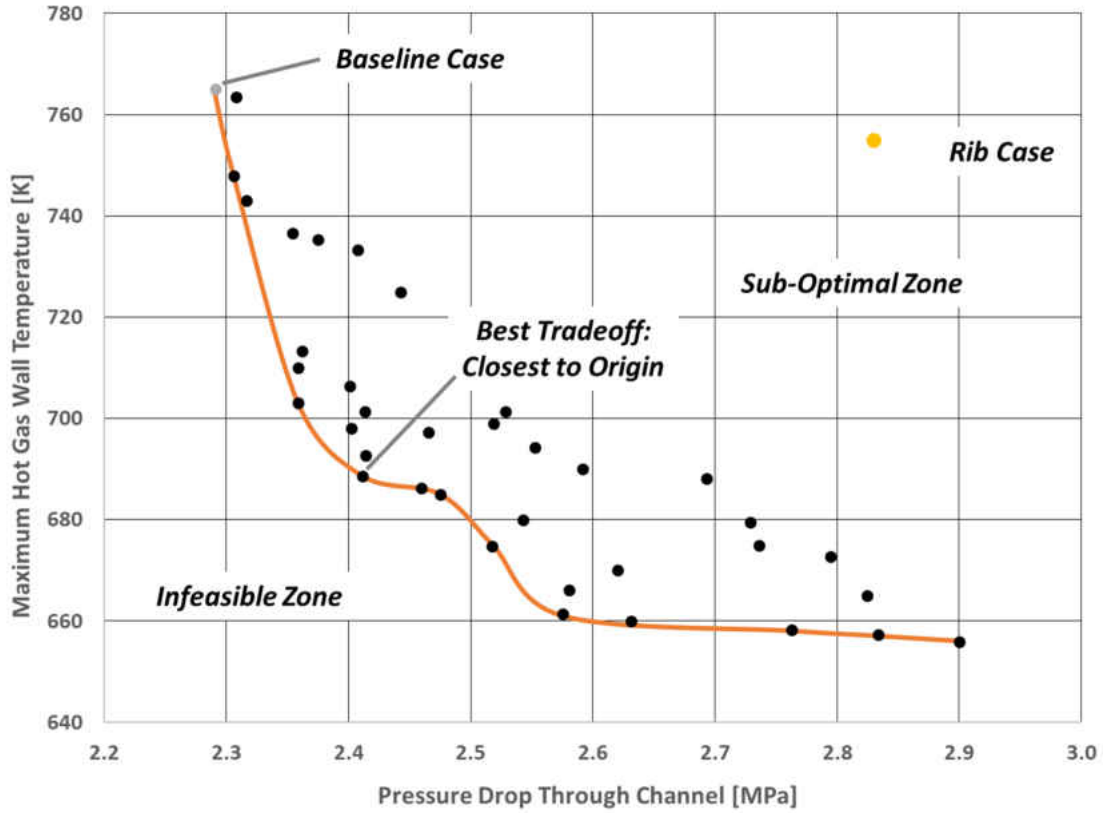
**Figure 58: Feasibility Front Results Obtained by Analysis of Many Wedge Configurations**
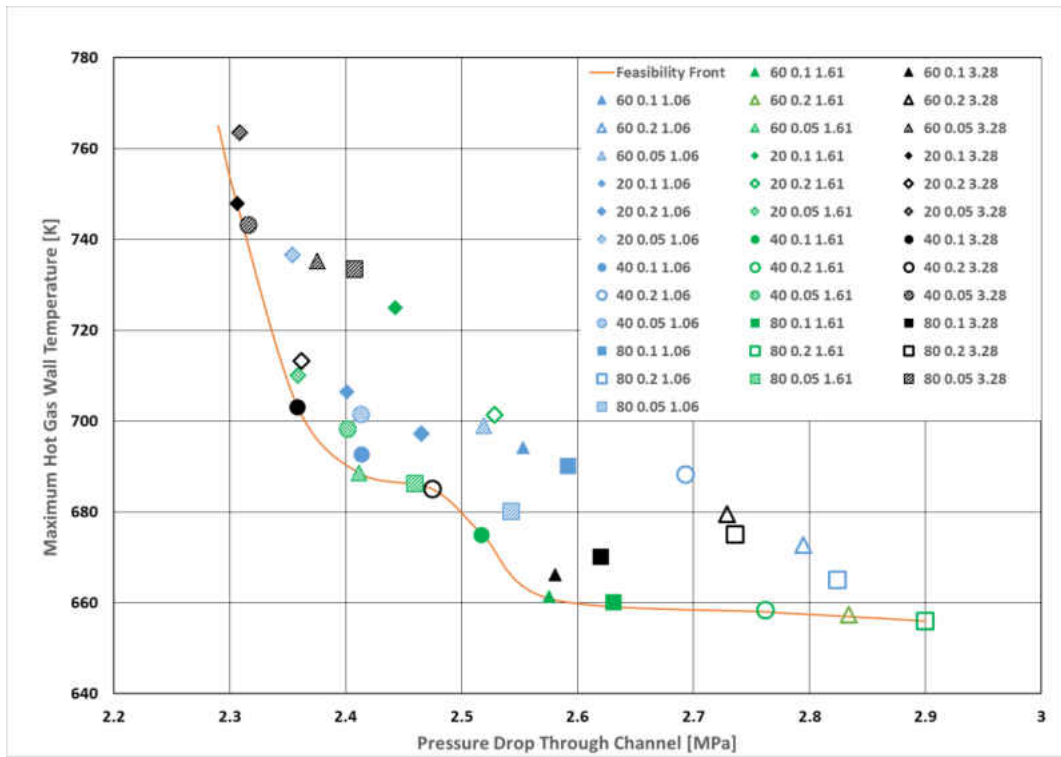


**Figure 59 Feasibility Front Results with All Wedge Cases Labeled**

Using the best tradeoff case, the low cycle fatigue can be determined for the potential use of wedges in LRE cooling channels. To start, the baseline maximum hot gas wall temperature is 765 K with the number of cycles to failure (based on equation 11) equal to 330. The best tradeoff case has a max hot gas wall temperature of 689 K and the number of cycles to failure is 549. This is a large increase in component life.

# CONCLUSIONS

The feasibility of using turbulators in a LRE cooling channel was investigated. The primary goal being to reduce the hot gas wall maximum temperature. A benchmark case for the present study was obtained from [2], and made into this study's baseline case. The hot wall flux from the baseline case was used as a boundary condition for all rib and wedge cases, to allow temperature to change and be compared from case to case. It is additive manufacturing techniques that allow the discussion of designing featured channels as small as those investigated in the current study.

The addition of ribs had little heat transfer enhancement effects and only served to increase the pressure drop. The addition of wedges in the initial wedge configuration showed that the heat transfer can be greatly increased with for a given pressure drop. The multi-configuration wedge study showed the thermal performance characteristics of many wedges configurations in this study's cooling channel. The greatest temperature reduction yielded a maximum hot wall temperature of 656 K with an associated pressure drop of 2.9 MPa. That configuration was with an 80-degree wedge, e/D.h of 0.2, and 49 (pitch of 1.61 mm) wedges in the channel. The point closest to the origin yielded a maximum hot wall temperature of 689 K with an associated pressure drop of 2.411 MPa. That configuration was with a 60-degree wedge, e/D.h of 0.05, and 49 wedges (pitch of 1.61 mm) in the channel.

The number of cycles to failure, based on low cycle fatigue correlations, increased from 330 for the baseline case to 549 for the best tradeoff case, which consists of a 60-degree wedge, e/D.h of 0.05, and a pitch of 1.61 mm (49 wedges in channel).

High aspect ratio channels from the baseline case investigator, Wadel et al, are more effective at heat transfer enhancement than the best tradeoff case in the current study. Wadel's best case yielded a hot gas wall max temperature of 618 K with an increase in channel pressure drop of 7.5%. The best tradeoff case from the current study yielded a hot gas wall max temperature of 689 K with an increase in pressure drop of 5.0%. Additional parameter changes such as mass flow rate, aspect ratio, sidewall thickness, etc, may improve the thermal performance of using wedges.

# FUTURE WORK

Based on the current study, there are beneficial paths for continuing investigations into improving their thermal hydraulic performance of LRE cooling channels. Some of those include:

- Performing a study with similarly shaped wedge turbulators in a similar LRE cooling channel, and impose an improved boundary condition. Instead of imposing a constant heat flux on the hot gas wall, the combustion environment should be simulated to determine the magnitude of the hot gas wall temperature decrease.

- A study with wedged turbulators should be performed with the goal comparing turbulator performance of a fixed geometry wedge, but with variable aspect ratio channels. This will have a large impact on the performance of the turbulator features.

- A study should be done with focus on the system level. To this end, a turbulator featured channel should be analyzed while changing parameters such as mass flow rate through the channel, the number of channels, varying pressure inlet or outlet conditions, and varying temperature inlet conditions. This study can reveal whether an optimal balance of all these parameters exists.

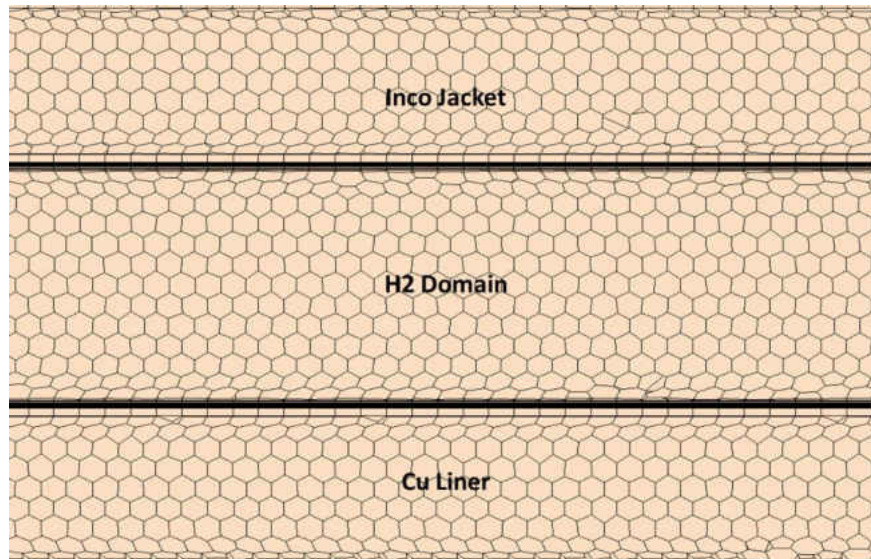- Printing a channel or channels for experimental study serves to verify and correct existing models.
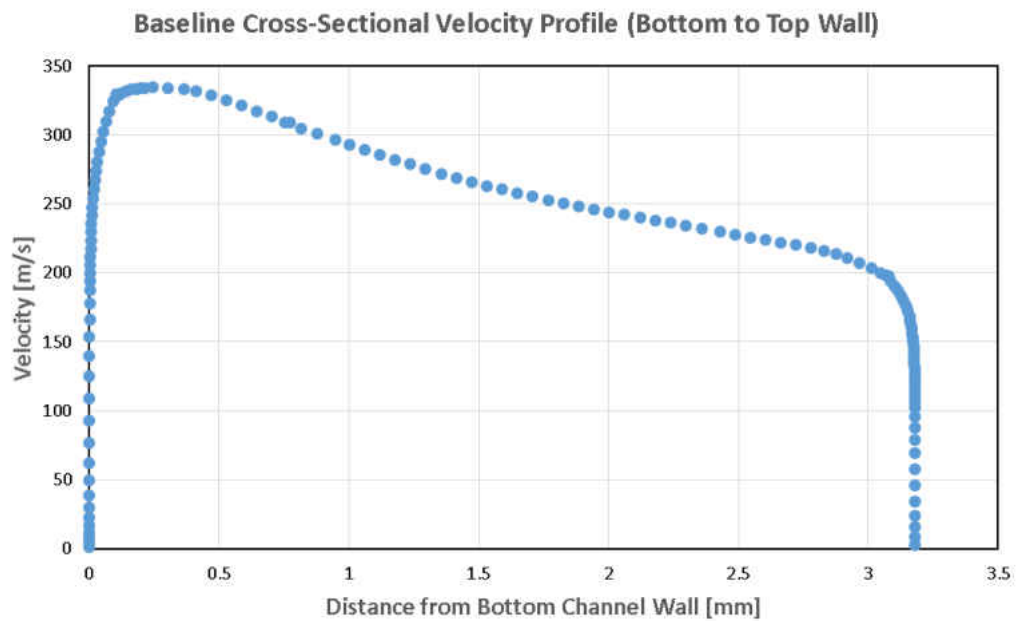
APPENDIX: MESH IMAGES
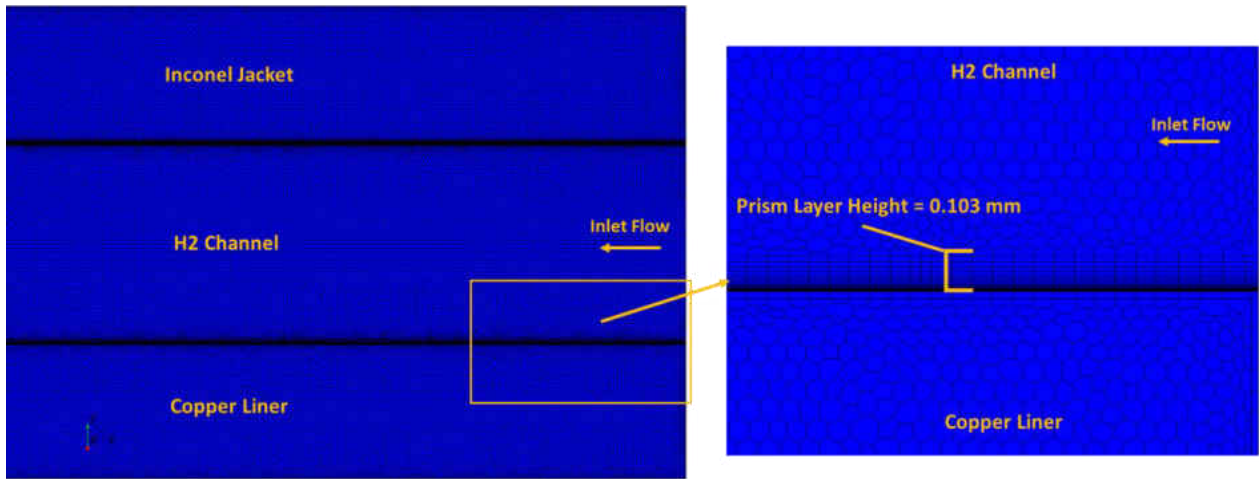
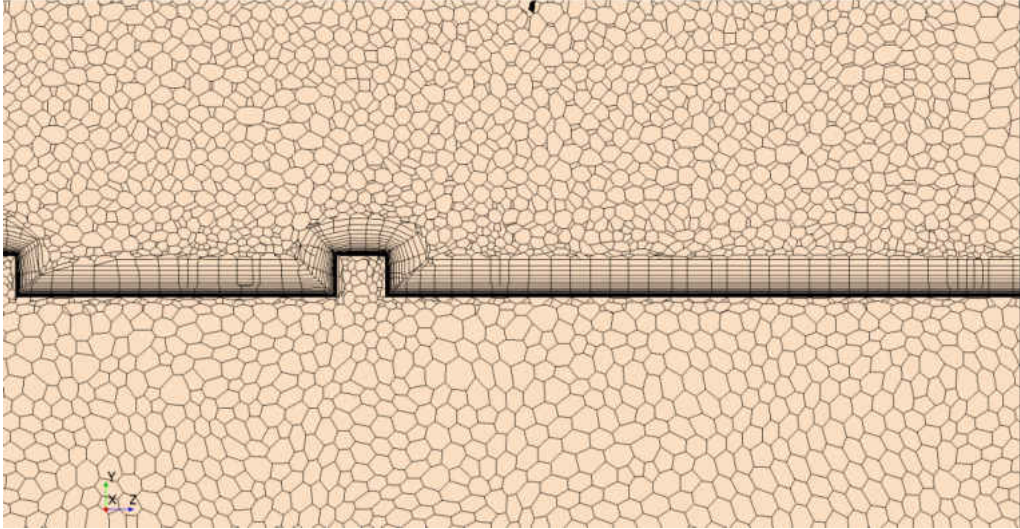**Figure A.1: Baseline Mesh 1, Midplane Near Inlet**
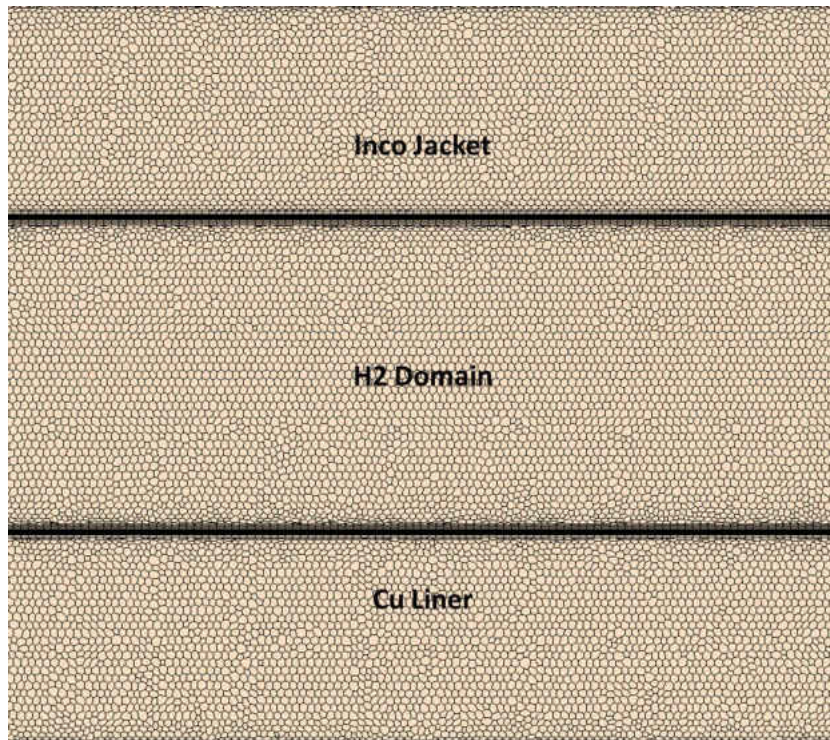
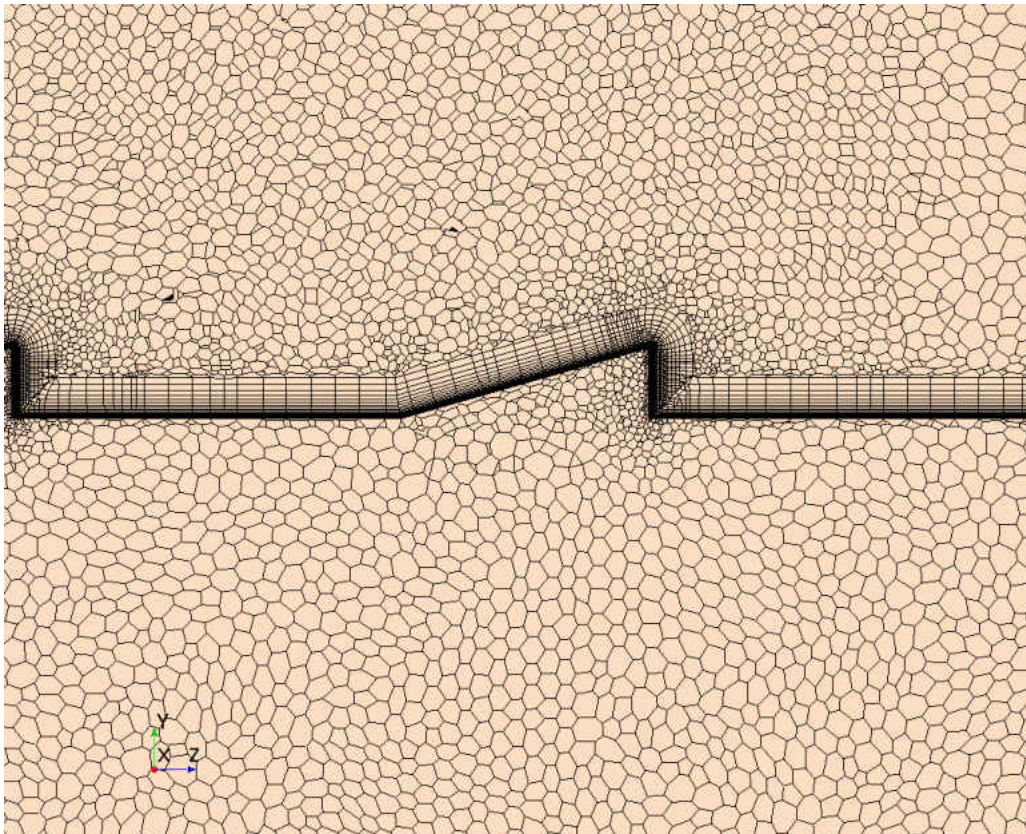

**Figure A.2: Baseline Mesh 2**

**Figure A.3: Baseline Mesh 3**



**Figure A.4: Baseline Cross-Sectional Velocity Profile**

**Figure A.5: Rib Case Mesh Midplane Side View near ribs**



**Figure A.6: Initial Wedge Case Mesh Midplane Side View near Wedges**

# REFERENCES

[1]  Garner, Rob. "Dr. Robert H. Goddard, American Rocketry Pioneer." *NASA*, NASA, 11 Feb. 2015, www.nasa.gov/centers/goddard/about/history/dr_goddard.html.

[2] "Turnaround Operations and Maintenance." *Space Shuttle Main Engine Pocket Data*, by Rockwell International, Rockwell International, 1987. RI/RD87-142.

[3] Image by Duk, distributed under a CC-BY 2.0 license.

[4] Sippel, Martin, et al. "Studies on Expander Bleed Cycle Engines for Launchers." 39th AIAA/ASME/SAE/ASEE Joint Propulsion Conference and Exhibit, 2003, doi:10.2514/6.2003-4597.

[5] Rajagopal, Manikanda. "Numerical Modeling of Regenerative Cooling System for Large Expansion Ratio Rocket Engines." Journal of Thermal Science and Engineering Applications, vol. 7, no. 1, 2014, p. 011012., doi:10.1115/1.4028979.

[6] Quentmeyer, R J. "Experimental fatigue life investigation of cylindrical thrust chambers." American Institute of Aeronautics and Astronautics, 13th Propulsion Conference, ed, 1977.

[7] Pizzarelli, Marco. (2017). Regenerative cooling of liquid rocket engine thrust chambers. 10.13140/RG.2.2.30668.92804.

[8] Lakshminarayana, Budugur. Fluid Dynamics and Heat Transfer of Turbomachinery. J. Wiley and Sons, 1996.

[9] Incropera, Frank P., and David P. DeWitt. Fundamentals of Heat and Mass Transfer. 7th ed., Wiley.

[10] Xometry.com. (2018). DMLS | Direct Metal Laser Sintering | Metal 3D Printing - Xometry. [online] Available at: https://www.xometry.com/direct-metal-laser-sintering.

[11] Harbaugh, Jennifer. "NASA 3-D Prints First Full-Scale Copper Rocket Engine Part." *NASA*, NASA, 21 Apr. 2015, www.nasa.gov/marshall/news/nasa-3-D-prints-first-full-scale-copper-rocket-engine-part.html.

[12] Wadel, Mary, and Mary Wadel. "Comparison of high aspect ratio cooling channel designs for a rocket combustion chamber." 33rd Joint Propulsion Conference and Exhibit, June 1997.

[13] Ulas, A., and E. Boysan. "Numerical Analysis of Regenerative Cooling in Liquid Propellant Rocket Engines." Aerospace Science and Technology, vol. 24, no. 1, 2013, pp. 187–197., doi:10.1016/j.ast.2011.11.006.

[14] Hossain, J, et al. "Numerical Study of Enhancement of Regenerative Cooling Using Ribs." 49th AIAA/ASME/SAE/ASEE Joint Propulsion Conference, Dec. 2013, doi:10.2514/6.2013-3996.

[15] Han, J. C. "Heat Transfer and Friction in Channels With Two Opposite Rib-Roughened Walls." *Journal of Heat Transfer*, vol. 106, no. 4, 1984, p. 774., doi:10.1115/1.3246751.

[16] Han, J.c., and Y.m. Zhang. "High Performance Heat Transfer Ducts with Parallel Broken and V-Shaped Broken Ribs." International Journal of Heat and Mass Transfer, vol. 35, no. 2, 1992, pp. 513–523., doi:10.1016/0017-9310(92)90286-2.

[17] Han, Je-Chin, et al. "Augmented Heat Transfer in Square Channels with Wedge-Shaped and Delta-Shaped Turbulence Promoters." Journal of Enhanced Heat Transfer, vol. 1, no. 1, 1993, pp. 37–52., doi:10.1615/jenhheattransf.v1.i1.40.

[18] Valentino, Michelle, et al. "Comparison of Heat Transfer and Friction Augmentation for Symmetric and Non-Symmetric Wedge Turbulators on Two Opposite Walls." 47th AIAA/ASME/SAE/ASEE Joint Propulsion Conference &Amp; Exhibit, 2011, doi:10.2514/6.2011-6021.

[19] Henze, M., et al. "The Effects Of Vortex Structures On Heat Transfer And Flow Field Behind Multielement Arrays Of Vortex Generators." Heat Transfer Enhancement, 2006.

[20] M. Peric and S. Ferguson, "The advantage of polyhedral meshes," CD-adapco< http://www. cd-adapco. com/press_room/dynamics/24/testVspoly. html, 2005.

[21] STAR-CCM+ User Guide, Mesh Metrics," https://stevedocs.cd-adapco.com/starccmplus_latest_en/index.html#page/STARCCMP%2FGU ID-733A3104-A053-47A1-AD86-8B16F4E4757B%3Den%3D.html.

[22] I. B. Celik, U. Ghia, and P. J. Roache, "Procedure for estimation and reporting of uncertainty due to discretization in {CFD} applications," Journal of fluids {Engineering-Transactions} of the {ASME}, vol. 130, 2008.

[23] "NIST Reference Thermodynamic and Transport Properties -- REFPROP."